Exploring The Two-Charge Holographic Superconductor

Barbera, Luca

Exploring The Two-Charge Holographic Superconductor

Thesis

submitted in partial fulfillment of the
requirements for the degree of

Master of Science
in
Physics

Author :	Luca J. Barbera
Student ID :	s3705439
Supervisor :	Prof. Dr. Koenraad Schalm
Daily Supervisor :	Dr. Nicolas Chagnet
Second corrector :	Dr. Subodh P. Patil

Leiden, The Netherlands, June 27, 2024

Exploring The Two-Charge Holographic Superconductor

Luca J. Barbera

Huygens-Kamerlingh Onnes Laboratory, Leiden University
P.O. Box 9500, 2300 RA Leiden, The Netherlands

June 27, 2024

Abstract

AdS/CFT gives a framework for using calculations from a weakly curved gravitational theory to describe phenomena in strongly correlated matter. In this work we study some holographic models this has put forward, such as the Reissner-Nordström metal and the holographic superconductor. Of these models we observe transport properties like the optical conductivity under both translational invariance and broken symmetry. Lastly, we merged the two systems into the two-charge holographic superconductor and managed to again see the phase transition, measure the optical conductivity and analyse the two-fluid model.

Contents

Version of June 27, 2024– Created June 27, 2024 - 01:41

Acknowledgements

I would like to sincerely thank the newly graduated Dr. Nicolas Chagnet for all his late night replies and spontaneous Sunday code-fixing sessions. I have learned so much from you, regarding holography, mathematics and numerics, but what has probably helped me the most over this time is that you believed in me when I myself was not able to. And no matter what you say, you are a great teacher.

Furthermore I am very happy that towards the end of my studies I got to experience what I think real research looks like. I appreciate all the weekly meetings we had and how professionally Koenraad guided us through this time. Even if I might not see myself in high energy theoretical physics in the future, I am very grateful of having had this experience. Not the last nor least of my thanks go to Aravindh, who always greeted me with a smile and made me feel at home in the institute.

These past two years at Leiden university have taught me much more than expected and opened up my mind to wonderful physical theories. And while LU has taught me a lot academically, it has also shaped my mind on what politics and communication I *do not* appreciate in a university and how I want to fight for a different approach.

Lastly, I want to thank Nina. From the very first problem set some seven years ago until the very last draft of my master's thesis, you have helped me in innumerable ways. This is truly the end of an era and I am excited to see what will come next for us.

Introduction

With the discovery of the weak-strong duality between classical gravitational systems and strongly interacting field theories in the large N-limit by Juan Maldacena [1] in 1997, he laid the foundation for classical computations of certain quantum mechanical systems where perturbative methods break down. This lead to Gubser, Klebanov, Polyakov [2] and separately Witten [3] in 1998 to come up with a dictionary translating interpretations and calculations from the gravitational to the field theoretical side and vice versa. Consequently, the holographic duality of condensed matter systems became an intense field of study with breakthroughs of describing strongly correlated matter such as the quark-gluon plasma (QGP) [4] for which there was no adequate model at the time.

The discovery of the holographic version of a superconductor by Hartnoll, Herzog and Horowitz (HHH) [5] sparked hope for finally going beyond the BCS theory of superconductivity. This way, many gravitational models dual to condensed matter systems were proposed that could one way or another describe the temperature, chemical potential, transport properties and more, of strongly correlated systems. Holography also sparked hope in being able to explain the right scaling behaviour of the optical conductivity [6–8] of strange metals by introducing holographic lattices that account for momentum dissipation in the system. Even though to date the right scaling was not able to be reproduced, the translational symmetry breaking that comes with holographic lattices is a key ingredient in investigating quantum critical points, cf. metallic systems [9, 10].

Further reassurance was gained by the ability of describing black hole hydrodynamics using holography. The analytical derivation of the correct viscosity-entropy ratio of a black hole [11] is only one example.

Studying holographic systems is a wonderful way to get a crash course in some of the most advanced and some of the most fundamental theories in physics. It is fascinating to see general relativity, quantum field theory, statistical physics and condensed matter systems in general and the rather old theory of hydrodynamics intertwined in such a way. One can make use of the recent advances in numerical GR [12] to model numerically heavy systems [13, 14] and use the holographic duality to understand strongly correlated systems.

This work is separated in four parts, of which the first gives the purely theoretical basis, such that the following three do hands-on calculations and extensions to the theory. The first chapter gives a brief overview of the AdS/CFT correspondence and the GKPW dictionary, before introducing the condensed matter transport property of optical conductivity and its field theoretical equivalent.

The second chapter mainly investigates the Reissner-Nordström metal and checks its

transport properties [8, 15]. This is where we first encounter numerics in holography and what we can expect from them. The following chapter introduces the HHH model of holographic superconductivity and measures the relaxed optical conductivity, recreating the holographic two-fluid model [16].

The fourth and final chapter combines all preceding systems, creating the two-charge holographic superconductor. The impact of the superconducting phase transition on an RN metal is tested and the foundation for further advancement in this direction is laid out.

Version of June 27, 2024– Created June 27, 2024 - 01:41

Chapter 1

A brief theoretical overview

1.1 AdS, CFT and The AdS/CFT correspondence

There is a surprising correspondence between general relativity and strongly coupled systems, where the former can be used to restate insights of the latter. Even though the unification of the two great theories of modern physics developed in the 20th century – general relativity and quantum field theory – has been troubling theoretical physicists for many decades now, viewing them as two sides of the same coin, as two systems *dual* to each other, has been discovered [1] to be a powerful tool in understanding strongly coupled matter. While perturbative treatments of quantum field theories using Feynman diagrams are extremely useful for weakly coupled systems, there are few computational tools to fully describe strongly coupled systems. The so-called AdS/CFT duality which is at the heart of this investigation holds specifically for *weak* classical gravity (which in turn is a special low energy case of supergravity [17]) and *strongly* coupled quantum field theories. So on one side we have an effective low energy field theory we understand well, whose dynamics are governed by Einstein's equations and have been solved in many different circumstances. On the other side we have problems that are practically impossible to describe by existing field-theoretical models. The correspondence between AdS (Anti-de Sitter spacetime) and CFT (conformal field theories) also goes by the title *holographic duality* or *gauge gravity duality*. In detail, these names address different aspects of the same theory. Strictly speaking we are never going to consider pure AdS spacetimes or truly conformal field theories. Naming it *holography* only comes from the fact that the gravity theory lives in one dimension higher than the quantum field theory describing the condensed matter system. For our purposes, however, it will work to use the three titles interchangeably.

The term *gauge-gravity* probably addresses the most general principle of the duality: it states that there is a connection between some gravity theory and a gauge field theory. As most (all) of the interesting cases are not in pure AdS, this title would be more accurate than AdS/CFT. In practice, these conventions just give us a variety of expressions to describe the same computational tool.

1.1.1 Conformal field theories

But why look at QFTs and more specifically, CFTs, in the first place? Quantum field theories are fundamental for the standard model of physics, they describe the weak, strong and electromagnetic interactions and have been backed by countless experiments. Conformal field theories are the subgroup of quantum field theories which are invariant under transformations that preserve angles. In particular, this includes special relativistic transformations (Poincaré transformations) and, most importantly, rescaling [18]. At first glance, scale invariant theories do not seem to occur often in nature. Most physical processes we know highly depend on the resolution at which a system is observed, or in other words, on the energy scale at which they are probed. Observing water on a bucket-scale, where the dynamics are governed by the Navier-Stokes equation is very different to describing the atoms that make up the water molecules on a quantum mechanical level, which happens at much smaller lengths and much higher energy scales.

So where is the connection to scale invariant theories? Sticking to the example of water, we observe a second order (i.e. continuous) phase transition through a critical point from liquid to vapour and we know from statistical physics that a system becomes scale invariant when approaching a critical point. More specifically, the correlation of degrees of freedoms e.g. the spin of two neighbouring electrons is just as strong as correlation between electrons far apart in the system – in other words, the correlation length becomes infinite [19]. This means that close to a critical point, any system will resemble a scale invariant system and a conformal field theory will be the right tool to describe its processes. This extends to quantum critical points (QCP) where phase transitions occur at zero temperature and whose observables AdS/CFT tries to explain.

1.1.2 Anti-de Sitter Space

Forgetting momentarily about the duality, let us first look at AdS_{d+2} and its properties. It comes as the unique solution to the Einstein-Hilbert action [20],

$$S = \frac{1}{2\kappa^2} \int d^{d+2}x \sqrt{-g} \left(R - 2\Lambda \right) \tag{1.1}$$

where $g = \det g_{\mu\nu}$. We select a certain negative cosmological constant such that it is related to the spatial dimensions d of the boundary theory

$$\Lambda = -d(d+1)/2L^2, \tag{1.2}$$

L being the AdS radius with dimension of length. The weak-strong duality we have hinted at, actually makes higher order derivatives in the action impossible and therefore the simple approach up to second order derivatives contained in the fully contracted Ricci scalar R is the right choice. A positive cosmological constant would lead to the famous de Sitter spacetime of constant positive curvature, modelling among other things an expanding universe [21].

Without other (matter) fields, the equations of motion describing the dynamics of the spacetime as a field (Einstein Equations) that are derived from this action are

$$R_{\mu\nu} = -\frac{d+1}{L^2} g_{\mu\nu}. \tag{1.3}$$

A metric that solves these equations is

$$ds^2 = \frac{r^2}{L^2}(-dt^2 + dx_i dx^i) + \frac{L^2}{r^2}dr^2 \tag{1.4}$$

$$\tag{1.5}$$

or with $r = L^2/z$

$$ds^2 = \frac{L^2}{z^2}(-dt^2 + dx_i dx^i + dz^2). \tag{1.6}$$

such that $r, z \in [0, \infty)$. We will stick to the latter parametrisation, as it will be favourable when doing numerics later on. The solution Eq. (1.6) is invariant under simultaneous rescaling of

$$z \to \lambda z \text{ and } x^\mu \to \lambda x^\mu, \tag{1.7}$$

and clearly maintains the Lorentz invariance of the Minkowski metric. The metric therefore exhibits isometries that are the same as a CFT. Greek indices label the $d+1$ spacetime dimensions $(-, +, +, ..)$ and the additional dimension z is labelled separately. The AdS curvature scale $1/L$ needs to stay small in Planck units in order to keep quantum gravitational effects negligible and for the duality to hold [9].

1.1.3 AdS/CFT correspondence

As mentioned before, the gravity theory needed for this duality to work, needs to be defined in one more dimension than the field theory it is dual to. Let us see where this additional dimension comes from. One can get from a microscopic field theory of small distances and high energies to one over long distances by integrating out degrees of freedom of the microscopic theory. Take a series of springs connecting masses: instead of considering each spring and mass individually, one can zoom out, or *coarse grain*, and average over multiple spring constants and masses. What one gets is an effective (field) theory describing the same system but from farther away – which is equivalent to probing at lower energies. So the same underlying system leads to theories with different coupling constants depending on the energy scale. What this means is that we actually see new physics *emerge* at different probing energies and we therefore need different theories at different scales.

The duality makes use of the fact that when we continuously change the energy scale of our field theory and *stick together* all these theories, we find that the emerging manifold can be described by classical general relativity. The way in which the field theory changes coupling constants is *geometrised* in the curvature of this emergent manifold. One can think of the field theory as constituting the high energy (UV) boundary of this curved space. And seen the other way around, the curvature in the interior of our spacetime encodes for what is happening in the field theory at low energies. The additional coarse-graining, holographic or *renormalisation* dimension can then be used to translate from the gravity theory into the boundary field theory. There is no sure fire way to construct an analogy that can fully explain this, but images like the ones in [13, 22, 23] help in getting an intuition for what is physically happening.

This *renormalisation* process is in our case labelled by the extra coordinate z. Energies are lower (infrared: IR) for higher values of z and vice versa. The boundary field theory lives at high energies ($z \to 0$) and we say that it is the UV limit of our *bulk* gravity theory in the interior.[1]

If we picture moving from a certain spacetime asymptotically into a boundary region that possesses the symmetries of a CFT, it is only logical to expect these same symmetries from the spacetime, too. This means that conformal transformations (inversion, rescaling, Poincaré) need to be reflected in the geometry of a spacetime capable of building this link. As a matter of fact, there is exactly one unique solution [17] for a metric of Minkowskian signature with $d+1$ spatial and one time component that preserves conformal symmetries: Anti-de Sitter spacetime.

We can count ourselves lucky that we are only looking to use AdS as a *computational* tool for describing strongly correlated matter and that we are not in need of a *real* AdS spacetime – as it does not describe anything of significance in our universe. Furthermore, it is important to comment, that this does not describe actual gravity that somehow interacts with a sort of metal or a field theory in a lower dimension. This is rather a whole new mathematical framework, derived from string theory, to bypass difficulties posed by strongly coupled quantum matter systems and instead use the libraries of knowledge we have on solving problems in Einstein gravity. Classical Einstein gravity is a special case of supergravity for weak curvature and low energies [23]. In the limit of a field theory of infinite flavours, this classical theory is capable of describing many physical phenomena of strongly coupled matter and is therefore an indispensable tool in describing high temperature superconductors and strange metals.

1.2 The AdS/CFT dictionary

The duality is powerful due to a *dictionary* translating observables from gravity to the field theory side and vice versa. One uses the so-called GKPW-dictionary [2, 3] named after Gubser-Klebanov-Polyakov and Witten to *shine through the CFT boundary to map to the holographic interior gravity theory*, as one would create a hologram in real life. What this means in practice is that we do need concrete prescriptions and formulas that allow us to express quantities on the field theory side via objects we describe our gravitational theory with. The construction can be strictly top-down from string theory, or it can be engineered manually from the bottom up, in order to get the observables wanted.

We will pick and present those entries that will be of use in our approaches, that is, we will take the translations as *axioms* that can be taken for granted. In the following sections of this introductory chapter we will motivate – yet not try to prove – the last three items. Works that introduce them properly and in different circumstances include [9, 10, 22, 24], and, rigorously in string theory [1]. The collection of GKPW dictionary entries we will work with is as follows:

1. The large N limit of a strongly coupled field theory can be described by a classical (weak curvature) gravity theory.

[1] We will use UV, boundary, field theory and IR, bulk/interior, gravity theory interchangeably in their respective regimes.

Version of June 27, 2024– Created June 27, 2024 - 01:41

2. The boundary of a $d+2$-dimensional gravity theory gives the background fields of a $d+1$-dimensional field theory. For example, the bulk metric for $z \to 0$ will be the spacetime of the field theory.

3. AdS curvature geometrises the renormalisation group flow, or "RG=GR"[9].

4. Local gauge symmetries of the bulk correspond to global symmetries on the boundary: The boundary value of a $U(1)$ gauge field in the bulk field therefore sources the conserved current associated with the global $U(1)$ of the field theory.

5. Fields in the bulk are said to be dual to (relevant) operators in the boundary. More specifically, the boundary value of a field in the gravity theory can be identified with the source of its dual operator in the field theory.

6. The leading behaviour of a bulk field is identified with the source of the corresponding boundary operator. The sub-leading behaviour is identified with its response, with its vacuum expectation value. In other words, the sources of the field theory set boundary conditions for fields in the bulk.

7. A black hole in the bulk gravity theory corresponds to a field theory at non-zero temperature, see section 1.2.1.

8. Adding a charge to the black hole furthermore introduces matter to the field theory, see section 1.2.2.

9. The scaling dimension of an operator on the boundary is connected to the mass of its dual bulk field, see section 1.2.3.

1.2.1 AdS-Schwarzschild Black Hole: introducing Temperature

Pure AdS_{d+2} in Eq. (1.6) does not allow for much to happen, we are thus going to perform the simple perturbation: breaking scale and Lorentz invariance in the bulk by setting $g_{tt} = -1/g_{zz}$. One example of this is the black hole Ansatz

$$ds^2 = \frac{1}{z^2}\Big(- f(z)dt^2 + dx_i dx^i + \frac{dz^2}{f(z)}\Big), \tag{1.8}$$

that solves both a Schwarzschild- and Reissner-Nordström-type action as will be introduced later. The AdS radius L is not a length scale in the dual field theory [25] and can therefore set to be 1 in the following. To not lose scale invariance in our boundary field theory, it is important to always recover pure AdS at high energies, or in other words, that our metric is *asymptotically AdS*, i.e. $f(z \to 0) = 1$. In the case of the simple Einstein-Hilbert action Eq. (1.1), the emblackening factor $f(z)$ is

$$f(z) = 1 - \Big(\frac{z}{z_0}\Big)^{d-1}, \tag{1.9}$$

which clearly fulfils the required asymptotics. Furthermore, we note that it vanishes at z_0, leading to a coordinate divergence in g_{zz}. As per usual with the Schwarzschild metric,

we identify z_0 with the black hole horizon beyond which nothing can escape anymore. We can analytically continue the metric to Euclidean time $\tau = it$

$$ds^2 = \frac{1}{z^2}\Big(f(z)d\tau^2 + dx_i dx^i + \frac{dz^2}{f(z)}\Big), \tag{1.10}$$

go to polar coordinates $\{\rho^2 = \alpha(z - z_0),\, \varphi = \beta\tau\}$

$$ds^2 = \frac{1}{(\rho^2/\alpha + z_0)^2}\Big(\frac{f(\rho)}{\beta^2}d\varphi^2 + \frac{4\rho^2 d\rho^2}{\alpha^2 f(\rho)} + dx_i dx^i\Big) \tag{1.11}$$

$$\tag{1.12}$$

and expand around $\rho = 0$

$$ds^2 \approx \frac{4}{z_0 \alpha f'(z_0)}\Big(\frac{f'(z_0)^2}{4\beta^2}\rho^2 d\varphi^2 + \frac{d\rho^2}{\alpha^2 f(\rho)} + \dots\Big) \tag{1.13}$$

to lift the coordinate singularity in $f(z_0) = 0$. By realising the form of polar coordinates $d\rho^2 + \rho^2 d\varphi^2$ we read off the periodicity of imaginary time

$$\beta = \frac{|f'(z_0)|}{2} = 2\pi\frac{|f'(z_0)|}{4\pi} \text{ and thus } \tau \sim \tau + \frac{4\pi}{|f'(z_0)|}. \tag{1.14}$$

As is done for the partition function in statistical physics, we can interpret the period of Euclidean time as the inverse of a temperature, giving the Hawking temperature [9]

$$T = \frac{|f'(z_0)|}{4\pi}. \tag{1.15}$$

We have arrived at another important duality between AdS gravity and the boundary CFT: an AdS black hole corresponds to a conformal field theory at finite temperature. The steps above are of course just the derivation for a diagonal metric of the form of Eq. (1.8), but we will refer back to this solution frequently. In this simple case where temperature is the only scale, all non-zero temperatures are equivalent and there are only two physical states: $T = 0$ (no BH present) and $T > 0$ (BH present). This can be seen in particular, when rescaling $z \to z_0\, z$ such that z_0 drops out of the temperature Eq. (1.15) making the temperature independent of the radial horizon coordinate z_0. In this way, we can equivalently describe the theory at any non-zero temperature just by rescaling z. We will need to introduce another physical scale in order to be able to differentiate states at different temperatures.

Beyond the formal duality, we come to see that it is not a coincidence for precisely an object like a black hole to inherit the thermodynamic character of the theory. The second law of thermodynamics states that the entropy of a system at non-zero temperature must always increase and therefore that information is dissipating. The character of a black hole horizon being a threshold of no-return for all time-and like-light particles shows the same behaviour. Later we will see that this dissipating character of a black hole in the AdS bulk is central to the correspondence.

Temperature is the starting point for deriving and defining thermodynamical variables like the free energy and entropy for various gravitational models. So far, the field theory at temperature T, however, only describes systems in vacuum and we need to further modify the model to account for matter.

1.2.2 AdS-Reissner-Nordstrom Black Hole: Introducing density and scale

Next to temperature, some particles, that is, a non-zero charge density or, in other words, a conserved charge is apparent in most condensed matter systems we want to describe in the boundary field theory. This conserved charge *keeping track* of matter is implied by the global $U(1)$ symmetry governing the boundary system. Using the dictionary as listed above in section 1.2, we know that a global symmetry of the boundary corresponds to a local one in the bulk. This is why introducing the $U(1)$ gauge field A_μ to the bulk will encode for a conserved charge (chemical potential), or simply, for matter in the boundary. Furthermore, GKPW implies that the boundary value of the bulk gauge field sources the boundary charge current (operator): $A_t \leftrightarrow J_t = \rho$. To describe a theory of time-and space independent density, $A_t = A_t(r)$ can only depend on the holographic direction. One can think of an electrostatic potential pointing radially outwards through the boundary. Reminding us of the potential of an electric monopole residing in the interior, this requires a charge at the origin. We naturally think of promoting the Schwarzschild black hole to the charged version of a static black hole, the Reissner-Nordström black hole, in the interior, in order to unite temperature with non-zero density in the boundary.

To introduce the chemical potential, we start by setting up the system we will analyse further in chapter 2. We extend the gravity theory by the field strength $F = dA$ to get the Einstein-Hilbert-Maxwell action[2]

$$S_{\text{EHM}} = \frac{1}{2\kappa^2}\int d^{d+2}x\,\sqrt{-g}\left(R + \frac{d(d+1)}{L^2} - \frac{1}{4e}F_{\mu\nu}F^{\mu\nu}\right), \tag{1.16}$$

where $3 = \frac{d(d+1)}{2}$ comes from the AdS_{2+2} cosmological constant and $R_{\mu\nu}$ and R are the Ricci tensor and the fully contracted Ricci scalar, respectively. From this we get the equations of motion for $g_{\mu\nu}$ and A_μ as

$$R_{\mu\nu} - \frac{1}{2}Rg_{\mu\nu} - 3g_{\mu\nu} = \frac{1}{2}T^{\text{EM}}_{\mu\nu} \tag{1.17}$$

$$\nabla_\mu F^{\mu\nu} = 0, \tag{1.18}$$

where

$$T^{\text{EM}}_{\mu\nu} = -\frac{2}{\sqrt{-g}}\frac{\delta S_{\text{EM}}}{\delta g^{\mu\nu}} \tag{1.19}$$

$$= \kappa^2(F_{\mu\gamma}F^{\gamma}_{\nu} - \frac{1}{4}g_{\mu\nu}F_{\beta\lambda}F^{\beta\lambda}). \tag{1.20}$$

A saddle point solution to the action above is still the metric Eq. (1.8), but now with altered emblackening factor

$$f(z) = (1-z)\left(1 + z + z^2 - \frac{\mu^2 z^3}{4}\right), \tag{1.21}$$

yielding the famous Reissner-Nordström (RN) solution of a static black hole with conserved charge. Here, we have already used scale invariance to set the black hole horizon

[2]Where e can be used to rescale the charge of the system.

to $z_0 = 1$, i.e. where f vanishes. This means that in the following we will be using units where the horizon sits at $z = 1$. The boundary naturally remains at $z = 0$. As dictated by GKPW, the bulk gauge field is constrained by the chemical potential μ in the boundary. In other words, the boundary value of the bulk gauge field sources the current density operator of the boundary. We tune the field theory to describe a system at μ merely by setting the boundary value to $A_t(z \to 0) = \mu$. We can immediately deduce another boundary condition that in turn follows from requiring regularity of $A^2 = g^{tt}A_t^2$ at the horizon. As $z \to 1$, the electrostatic potential A_t must vanish to counter the diverging emblackening factor $f(z \to 1) \sim g^{tt}$ in order to ensure regularity. Put together, this implies that the gauge field can be written as

$$A = \mu(1 - z)dt \text{ or, equivalently } A_t(z) = \mu(1 - z), \tag{1.22}$$

where by the dictionary we have that $-A_t'(0) = \mu = \rho$ is the response. The solution of $f(z)$ describing $g_{\mu\nu}(z)$ and $A_t(z)$ are the so called *background solution*. They are the simplest analytically available and static, yet meaningful solutions to the equations of motions and can be seen as the equilibrium solution. Later on, we will introduce further variables t, x, and y to include more effects into our model, but these will just be small perturbations deviations *around* the background. Therefore, the first step of every holographic model will be to analytically or, when necessary, numerically solve for these background fields.

We can deduce the scaling behaviour of μ and T when simultaneously rescaling $z \to \tilde{z} = \lambda z$ and $t \to \tilde{t} = \lambda t$: The physical tensor A does not rescale, therefore

$$A = A_t dt = A_t \frac{d\tilde{t}}{\lambda} = \tilde{A}_t d\tilde{t} = \tilde{A} \Rightarrow \tilde{A}_t = A_t/\lambda, \tag{1.23}$$

and with it also $\mu \to \mu/\lambda$. The same behaviour can be found for the temperature using[3] the Hawking temperature of Eq. (1.15) such that

$$T = \frac{\partial/\partial z f(z_0)}{4\pi} = \frac{\lambda \partial/\partial \tilde{z} \tilde{f}(\tilde{z}_0)}{4\pi} = \lambda \tilde{T} \tag{1.24}$$

or, equivalently, that $T \to T/\lambda$. As we identified in the previous chapter, all AdS-Schwarzschild theories that describe a non-zero temperature are equivalent. Having introduced another scale, the *quantity* of chemical potential, however means, that we can describe different physical states by looking at different values of the *ratio* of the two scales T and μ. More concretely, this means that we have a scale invariant, dimensionless quantity

$$\frac{T}{\mu} = \frac{\tilde{T}}{\tilde{\mu}} \tag{1.25}$$

uniquely defining the state of our system. In the following, the only physical results we can get from out calculations will be in these dimensionless units. Of course, the relation may change, as for example in the case of the charge density, which is only dimensionless in ρ/μ^2.

The Reissner-Nordström solution has been extensively studied [21] and a lot of insights can be readily transferred to its holographic counterpart. In the case of a large mass

[3] Scale invariance $ds^2 = d\tilde{s}^2$ of the metric implies $f(z) = \tilde{f}(\tilde{z})$ and it is obvious that $\partial/\partial z = \lambda \partial/\partial \tilde{z}$.

compared to the charge of the RN black hole, the charge can be neglected and we return to the regular Schwarzschild solution. In the gauge-gravity duality this corresponds to a theory at $T \gg \mu$, which is not what we are interested in. In the other extreme, $T < \mu$, on the other hand, describes a theory at finite density and low temperature with the lower bound of $T = 0$. This lower bound is exactly recovered [9] when using the appropriate Hawking temperature Eq. (1.15) in the case of an extremal AdS-RN black hole where its charge makes up all of the mass. In the language of black hole thermodynamics: the black hole's mass cannot possibly shrink by emitting Hawking radiation and without emission the temperature of the black hole must be zero. This describes a system at finite charge yet *zero temperature* and most importantly finite ground state entropy, forming a quantum critical point.

1.2.3 Two-point correlator and field-operator duality

One example for the bottom up approach is the construction of the two-point correlator

$$\langle O(x)O(0)\rangle = \frac{1}{|x|^{2\Delta}} \tag{1.26}$$

of a scalar observable $O(x)$ that scales in the conformal field theory as $O(\lambda x) = \lambda^{-\Delta}O(x)$. In Fourier space we can obtain the retarded correlator (cf. [9] chapter 5)

$$\langle O(k)O(0)\rangle \sim k^{2\Delta-d-1}. \tag{1.27}$$

Correlators of scalar, vectorial or tensorial operators are important observables of any CFT, as they can, as mentioned before, indicate phase transitions and (because) they encode (linear) response to small perturbations describing transport processes. So in order to engineer something that on the gravity side of things looks like the CFT-correlator Eq. (1.26), we naively start with adding some simple field to our gravity theory: A massive scalar field ϕ, minimally coupled to our AdS background via the action

$$S_\phi = -\frac{1}{2}\int d^{d+2}x\,\sqrt{-g}\Big(\partial_\mu\phi\partial^\mu\phi + m^2\phi^2\Big). \tag{1.28}$$

Analogous to [9] chapter 1, we Fourier transform the subsequent equation of motion

$$(\nabla_\mu\nabla^\mu - m^2)\phi = \frac{1}{\sqrt{-g}}\partial_\mu(\sqrt{-g}g^{\mu\nu}\partial_\mu\phi) - m^2\phi = 0 \tag{1.29}$$

in all non-holographic dimensions, i.e. $\{x^\mu, z\} \to \{k^\mu, z\}$ (of which $x^0 = t = i\tau$ and $k^0 = \omega = -i\omega_E$ in imaginary time and frequency)

$$\hat{\phi}_k''(z) - \frac{d}{z}\hat{\phi}_k'(z) - \Big(k^2 + \frac{m^2}{z^2}\Big)\hat{\phi}_k(z) = 0. \tag{1.30}$$

It is important to notice, that this expression can be redefined in $\zeta = z\,k$, such that the solution is a function solely of ζ. This is a first hint to why we can think of the renormalisation dimension as an (inverse) energy scale.

As we proposed the field theory to live on the UV boundary of the gravity dual, we observe the field's dynamics close to the boundary $z \to 0$ and see that up to leading order the Fourier amplitude behaves as

$$\hat{\phi}_k(kz) = z^{d+1-\Delta}\Big[A(k) + \mathcal{O}(kz)\Big] + z^{\Delta}\Big[B(k) + \mathcal{O}(kz)\Big], \tag{1.31}$$

where

$$\Delta = \frac{d+1}{2} + \sqrt{\frac{(d+1)^2}{4} + m^2 L^2} \tag{1.32}$$

and $A(k) = a\, k^{d+1-\Delta}$ and $B(k) = b\, k^{\Delta}$. For certain values of Δ, the first term happens to be non-normalisable, while the second term is by definition normalisable. Following the GKPW dictionary, we see that the leading order coefficient $A(k)$ can be seen as the source of the dual boundary operator and the sub-leading $B(k)$ as the response to it, that is, the vacuum expectation value of the dual operator. Here we finally recover what we were looking for: we constructed an observable on the gravity side that scales the same way in momentum k as our two-point correlator of Eq. (1.27) on the CFT side:

$$\frac{B(k)}{A(k)} \sim k^{2\Delta - d - 1} \tag{1.33}$$

when identifying Δ from Eq. (1.32) with the scaling dimension of the operator $O(x)$. Similar steps for different types of fields coupling to gravity can be taken in order to derive vectorial and tensorial correlators [26]. Now, by introducing the correct field into our gravity theory and extracting its (non-) normalisable leading order behaviour at the boundary, we can calculate the field theoretical correlator of the operator dual to the field.

1.3 Optical Conductivity and Drude Theory

Taking a step back from holographic duality, we need to look at the observable we aim to describe on the field theory side: the conductivity. It quantifies the response of a system to a small, externally applied perturbation. If the external field is small enough that the physical state of the system is not altered, the response can be seen as perturbative and therefore linear to the source of perturbation. We then get in linear response theory

$$J = \sigma E. \tag{1.34}$$

When the external field E is driven at a frequency ω, the density current J also depends on ω and we call $\sigma(\omega)$ the *optical conductivity*.

1.4 Drude Theory

Drude theory explains the conductivity based on particles scattering off impurities, a background lattice and in general interaction leading to scattering – see [8] or [27] for more detail. The lattice in particular implies breaking of the Galilean continuum and therefore describes systems with broken translational symmetry. The ability for the particles to

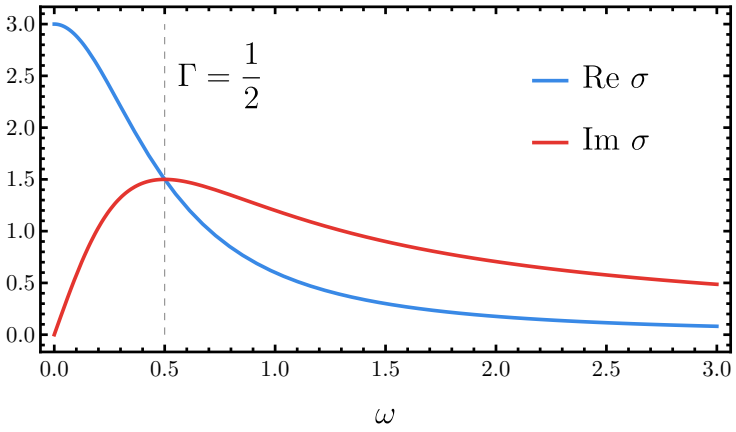

Figure 1.1: Drude theory optical conductivity. *The real and imaginary part of the optical conductivity $\sigma(\omega)$ as given by Drude theory Eqs.* (1.35)-(1.37)*. The width of* $\mathrm{Re}\,\sigma$ *and the position of the maximum of* $\mathrm{Im}\,\sigma$ *are given by the momentum dissipation rate* $\Gamma = 0.5$ *and the DC conductivity by* $\mathrm{Re}\,\sigma(\omega \to 0) = \sigma_0 = 3$.

scatter introduces momentum dissipation, as the particles can *dump* their energy into dissipative modes, just like waves rippling out from a stone thrown into water carry the stone's excess energy. The hydrodynamic analogy is especially accurate, as, for example, the Navier-Stokes fluid can be derived from the holographic bulk dynamics [9].

The resulting conductivity and its real and imaginary part are

$$\sigma(\omega) = \frac{\sigma_0}{1 - i\omega\tau} + \sigma_Q = \frac{\omega_p^2}{\Gamma - i\omega} + \sigma_Q \tag{1.35}$$

$$\mathrm{Re}\,\sigma(\omega) = \frac{\omega_p^2\,\Gamma}{\Gamma^2 + \omega^2} + \sigma_Q \tag{1.36}$$

$$\mathrm{Im}\,\sigma(\omega) = \frac{\omega_p^2\,\omega}{\Gamma^2 + \omega^2}, \tag{1.37}$$

where $\Gamma = \tau^{-1}$ is the rate of momentum dissipation and

$$\omega_p^2 = \sigma_0 \Gamma \tag{1.38}$$

the plasmon frequency. The frequency independent conductivity, the *DC* conductivity $\sigma(\omega \to 0) = \sigma_0$, is given by $\sigma_0 = nq^2/\Gamma m$ [8, 10]. The full optical conductivity $\sigma(\omega)$, the *AC* conductivity, is referring to the equivalent of an alternating current driving the external field. The real and imaginary parts of the conductivity are shown in Fig. 1.1. The low frequency regime $\omega \leq \Gamma$ dominated by the real part is described by a Lorentzian of the width Γ. This is the so-called *Drude peak* and a conductivity that shows such a peak at low frequencies is *Drude like*. At higher frequencies, the imaginary part dominates and the conductivity approaches that of free particles due to the strongly oscillating external field: the particle's direction is changed by the external field before it has time to interact with its surroundings [8]. The width of the peak Γ is directly proportional to the strength of translational symmetry breaking and the amount/intensity of momentum dissipation. Without dissipation of momentum, the density current is infinitely accelerated by the constant external field at $\omega = 0$ and the conductivity is described by a single δ-peak at zero frequency.

These relations and figures will be the reference as to how well the field theory we set up via the gravitational system will be able to reproduce the behaviour of a condensed matter system that can be described by Drude theory.

Optical conductivity of a field theory

Eventually, our goal will be to calculate the optical conductivity of our our field theory using the gravity side. In linear response theory, we obtain the conductivity via the Kubo formula [28] and the retarded Green's function G^R. When the external field is applied in y-direction, this takes the form

$$\sigma(\omega) = -\frac{i}{\omega} G^R_{yy}(\omega, \mathbf{k} = 0), \tag{1.39}$$

where in Fourier space the Kubo formula gives the retarded Minkowski space Green's function as the current-current correlator of the form

$$G^R_{yy}(\omega, \mathbf{k}) = -i \int dt d\mathbf{y}\ e^{-i(\omega t - \mathbf{k}\cdot\mathbf{y})} \Theta(t) \langle [J_y(t, \mathbf{y}), J_x(0, 0)] \rangle, \tag{1.40}$$

with $\Theta(t)$ the Heaviside function and J_y the density current in y-direction. To measure σ at non-zero $\mathbf{k}$ in the lab, the system would have to be probed with a non-zero wave vector, which is experimentally challenging and we can therefore set $\mathbf{k} = 0$ in Eq. (1.39).

So far we have covered basic principles of the AdS/CFT correspondence that will be relevant to us, their application to certain systems and Drude theory describing the linear response of a system to an externally applied field and how this can be calculated in a field theory. The following three chapters are going to each look at a different gravitational setup that is dual to some field theory describing strongly coupled matter. The first two chapters deal with well studied holographic systems such that we can use them to fill our toolbox and get used to the concepts involved. In the final chapter we will eventually set up a new *two-charge* system and find out its properties applying the methods studied before.

Chapter 2

The RN Metal

We have already seen that by introducing not only temperature, but also chemical potential duals to our gravitational theory, we have constructed a grand canonical field theory on the boundary that is capable of describing a metal. Following the GKPW dictionary for a weakly coupled gravitational theory, this constitutes a strongly coupled metal which are notoriously difficult to model. Of course strictly speaking, this describes not only a metal, but any field theory described by a conserved $U(1)$-charge. We are basically using the gravity theory to describe a field theory of *something* that does not vanish and whose currents are governed by a continuity equation. Speaking of a metal in the boundary paints a picture and eases the naming, as long as one keeps this in mind.

In the following chapters we will consider an AdS_{2+2} bulk, that is $d = 2$, including two spatial (x, y), one temporal t and the holographic z dimension. We can start off with the background solutions for the bulk fields $g_{\mu\nu}$ and A_μ obtained in section 1.2.2

$$ds^2 = g_{\mu\nu}dx^\mu dx^\nu = \frac{1}{z^2}\Big(- f(z)dt^2 + dx_i dx^i + \frac{dz^2}{f(z)}\Big) \tag{2.1}$$

$$f(z) = (1-z)\Big(1 + z + z^2 - \frac{\mu^2 z^3}{4}\Big) \tag{2.2}$$

$$A = \mu(1-z)dt \tag{2.3}$$

$$\tag{2.4}$$

that give the Hawking temperature of the RN black hole

$$T_{RN} = \frac{|f'(1)|}{4\pi} = \frac{12 - \mu^2}{16\pi}. \tag{2.5}$$

Here we can see that setting the boundary value of A_t, that is μ, controls the temperature of the boundary theory. The temperature therefore decreases for increasing μ and the chemical potential is bounded by absolute zero, i.e. $\mu < \sqrt{12}$. The background solutions are shown in Fig. 2.1. A_t is simply a straight line connecting the two boundary conditions and $f(z)$ is asymptotically 1 as demanded by the duality. Having set up a theory that can describe a metal, we should measure the optical conductivity to see whether it indeed behaves like a metal. At first, we will consider a translationally invariant model with a homogeneous boundary of constant μ to get a feel for linear response in this kind of system, such that later the more realistic case of translational symmetry breaking leading to dissipation of momentum can be recreated.

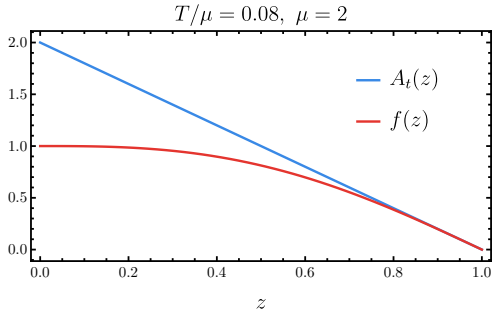

Figure 2.1: RN background solutions. *Background solutions for the RN metal at $\mu = 2$ and temperature $T/\mu = 0.8$ as functions of the holographic dimension z. The black hole horizon is at $z = 1$ and the UV boundary at $z = 0$. As demanded, the emblackening factor vanishes at the horizon and is asymptotically AdS. The gauge potential vanishes at the horizon and sources the density current by setting $\mu \neq 0$ at the boundary.*

2.1 Optical conductivity on a translationally invariant background

So how do we now calculate this optical conductivity using only the gravity theory? The GKPW dictionary from section 1.2 states that leading and sub-leading order of the bulk field corresponds to source and response of the dual boundary operator, respectively. Just as we showed in section 1.2.3, where the two-point correlator $\langle OO \rangle$ was derived as the ratio of sub-leading to leading order behaviour of ϕ, we will be able to get the $\langle J_y J_y \rangle$ correlator from Eq. (1.40) by the ratio of sub-leading to leading order in δA_y, analogous to chapter 7.3 in [9], as

$$\langle J^y(-\omega) J^y(\omega) \rangle \sim \frac{\delta A_y^{(1)}}{\delta A_y^{(0)}}. \tag{2.6}$$

In order to get a conductivity at finite frequency and zero wave vector, we perturb the background solution as

$$A_\mu \to A_\mu + \delta A_\mu(z,t) = A_\mu + a_\mu(z) e^{-i\omega t} \tag{2.7}$$

$$g_{\mu\nu} \to g_{\mu\nu} + \delta g_{\mu\nu}(z,t) = g_{\mu\nu} + h_{\mu\nu}(z) e^{-i\omega t} \tag{2.8}$$

where $|a_\mu|, ||h_{\mu\nu}|| \ll 1$. Here, we use the radial gauge $a_z = 0$ as this direction does not capture relevant physics. When focusing on the y-direction, we see that the dynamics of a_y only depend on the y-component of Eq. (1.18) and yz-component of Eq. (1.17). Perturbations h_{ty} and a_y decouple and we get a single second order ODE for the latter:

$$0 = a_y'' + \frac{f'}{f} a_y' + \frac{\omega^2 - z^2 A_t'^2}{f} a_y, \tag{2.9}$$

The near-boundary solution of this is of the form

$$a_y(z) = A + B\, z + \ldots, \tag{2.10}$$

where A, B are constants and the ellipsis denotes negligible higher orders in $z \to 0$. This in turn means, that the solution to Eq. (2.9) at the boundary gives the leading and its

derivative at the boundary the sub-leading order of our bulk field fluctuations, formally $A = a_y(0)$ and $B = a_y'(0)$. Via Eqs. (2.6), (1.40) and (1.39) we then get the optical conductivity of an RN metal

$$\sigma_x(\omega) = -\frac{i}{\omega}\frac{a_y^{(1)}}{a_y^{(0)}} = -\frac{i}{\omega}\frac{a_y'(z=0)}{a_y(z=0)}. \tag{2.11}$$

There is, however, some ambiguity in the process of defining the retarded Green's function in Eq. (1.40) and its relation to our *electromagnetic* waves $a_y(z)$ that we need to consider before solving for σ_y. We know from electrodynamics that the response to some source field travels at the speed of light, so that the response comes some time after the effect. Formally, there is also another solution, where the response precedes and travels towards the source, which is of course not a physical process we observe. The same ambiguity occurs with our AdS waves, as they can either travel towards the charged black hole or away from it. From the no-return character of the black hole horizon which is dual to the dissipation in a thermodynamic system, it follows, that solutions are only physical if they are *in-falling* into the black hole. In the following we must therefore select the boundary conditions that ensure regularity at the horizon and that solutions do not travel from inside the black hole towards the AdS-boundary but the other way around. Another way to ensure this would be to consider imaginary-time propagators on the boundary via a Wick rotation, as Euclidean Green's functions are uniquely defined and physical [29] such that regularity itself would be sufficient. As the whole imaginary time via Wick rotations introduce a lot of other difficulties, we will stick to the Minkowski space retarded Green's function.

Close to the horizon, the two solutions to Eq. (2.9) that dominate at leading order are

$$a_y(z) \sim (1-z)^{\pm\frac{i\omega}{4\pi T}}, \tag{2.12}$$

where "+" counts the outgoing and "−" the in-falling wave. This can be seen by choosing the Ansatz

$$a_y(z) = (1-z)^{\alpha} a_{\text{inf}}(z) \tag{2.13}$$

and demanding the leading order of Eq. (2.9) around the horizon to vanish. We then manually rescale $a_y(z) \to (1-z)^{-i\omega/4\pi T}\, a_{\text{inf}}(z)$ to ensure that the in-falling wave is selected and the sub-leading $a_{\text{inf}}(z)$ cannot lead to causality issues.

The procedure of how we set up and naively solved this system of coupled differential equations will be described in section 2.3. A more universal method using *gauge invariant variables* – the one that was finally used for most computations – will be presented for the final system in section 4.2. However, before going into detail on how to obtain them, let us look at the optical conductivities that we can calculate for this system.

2.1.1 Results

Numerically solving Eq. (2.9) for $a_y(z)$, while respecting infalling boundary conditions, finally gives the optical conductivities Figs. 2.2 and the temperature dependence of the *DC* conductivity Fig. 2.3.

Comparing to the curves in Drude theory, Fig. 1.1, we see that both real and imaginary part are not Drude-like. There is no Drude peak in the low frequency regime of the real

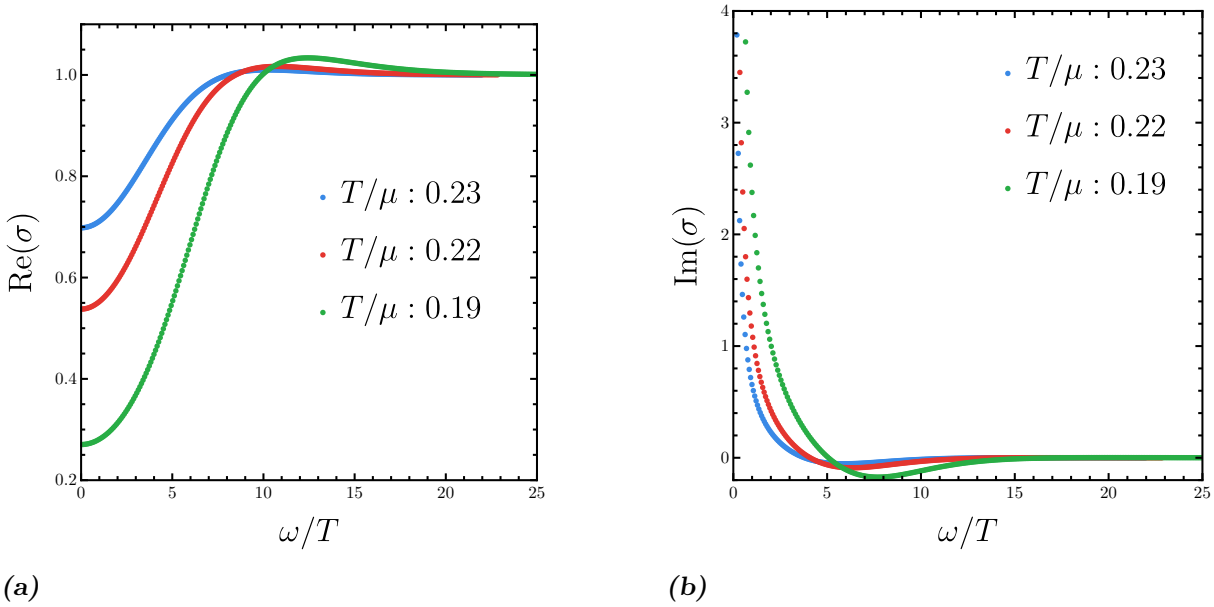

(a) **(b)**

Figure 2.2: Optical conductivity of the pure RN metal at different temperatures. *Real (a) and imaginary part (b) of the optical conductivity calculated for the pure RN system at temperatures $T/\mu = 0.23$ (blue), $T/\mu = 0.22$ (red), $T/\mu = 0.19$ (green). For all three temperatures there is no Drude peak in the low-frequency regime, as is expected by a translationally invariant system. For $\omega/T \gg 1$ all curves recover the zero density CFT value of $\mathrm{Re}\,\sigma = 1$. The declining spectral weight in of the real part is recovered in the imaginary part.*

part and the imaginary part seems to diverge. Only the high frequency asymptote of the real part seems to match our expectation. For $\omega/T > 1$ we expect the chemical potential to be negligible and the theory therefore to look like a CFT at zero density [8]. The high frequency conductivity of graphene measured by Li et al. [31], for example, looks very similar. The graphene measurements show, however, that there should also be a low frequency peak of finite width in the real part. We gain some insight about what is going wrong at $\omega/T < 1$ in Figs. 2.2 from the Kramers-Kronig relation[8] ensuring unitarity of our theory. The relation can be used to state that the divergent imaginary part $\sim 1/\omega$ is proof of a *hidden* δ-peak at zero frequency in the real part. This implies that our conductivity currently only describes a translationally invariant system that is described at low frequencies by the conductivity

$$\sigma(\omega) = \omega_p^2\left(\delta(\omega) - \frac{1}{i\omega}\right) + \sigma_Q, \tag{2.14}$$

which is basically the $\Gamma \to 0$ limit of Eq. (1.35), when we think of the real part turning from a Lorentzian into the invisible δ-peak.

The graph of 2.2(a) clearly does not start from the origin, there is some remaining conductivity σ_Q that is neither zero nor does it seem to belong to the hidden $\delta(\omega)$. Davison et al. [30] investigated this *universal conductivity* σ_Q, stating that it persists even in *clean* systems with conserved momentum and a non-zero particle density. It is a relativistic effect coming from gradient corrections to the current density. Being intrinsic to the system, it is not related to the externally applied field. Davison et al. derived a

Version of June 27, 2024– Created June 27, 2024 - 01:41

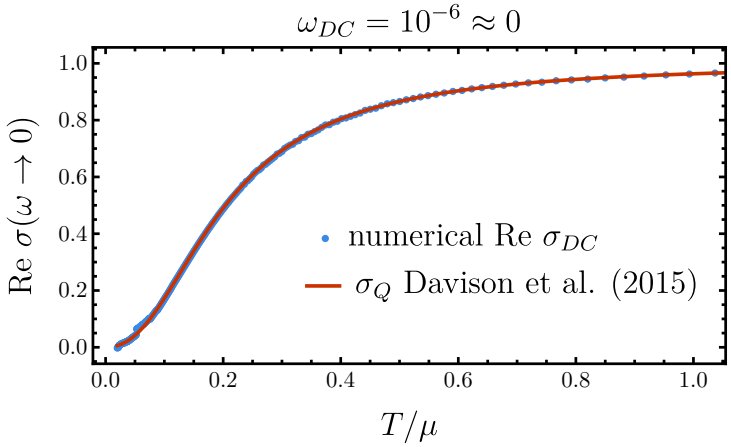

Figure 2.3: DC conductivity over temperatures $\mathbf{T}/\mu$. *The real part of the optical conductivity for* $\omega \to 0$ *increases with temperature, exactly following the trend of the universal conductivity* σ_Q *Eq.* (2.15) *found by Davison et al. [30].*

closed expression for σ_Q as

$$\sigma_Q = \left(\frac{sT}{sT + \mu\rho}\right)^2 = \left(\frac{\frac{12-\mu^2}{4}}{\frac{12-\mu^2}{4} + \mu^2}\right)^2, \tag{2.15}$$

where the latter is our case of $\rho = \mu$, $s = 4\pi$ and with the Hawking temperature of Eq. (2.5). Our data seems to verify this behaviour up to some small numerical error at very low T/μ as can be seen in Fig. 2.3. The DC conductivity decreases with the temperature, i.e. the spectral weight is being depleted. This depletion is compensated by the increase in the pole strength of the delta function at zero frequency.

As seen above, this model of a translationally invariant system does not account for dissipation of momentum. In order to recreate the correct Drude behaviour at small frequencies, we are going to break translational symmetry of the background in the following chapter.

2.2 Translational symmetry breaking via Axion

Clearly, we are able to reproduce some metallic phenomena at relative ease using our engineered gravity theory. Real world metals, however, consist of a lattice, explicitly breaking the translational symmetry that persists in our gravitational model. The holographic model lives in a Galilean continuum that needs to be discretised in order to mimic a real crystal. As mentioned before, the breaking of translational invariance will allow for electrons to dump their momentum into a bath, leading to their slowing down and a non-zero resistivity.

There are multiple ways to account for translational symmetry breaking in our current setup. The most direct way is to add a gravitational background lattice by promoting the homogeneous background chemical potential μ to a spatially modulated source $\tilde{\mu}(x) = \mu + A\cos(kx)$ as has been done by Horowitz et al. [6] in one and Balm et al. [14] in two spatial dimensions. The problem with this approach is, however, that the introduction of spatial dependence makes the equations of motion into a system of coupled *partial*

differential equations rather than ordinary ones as before, as we will come to see in section 2.4. The boundary conditions are not as straight forward and it is advisable to choose a specific gauge using the DeTurck method [23] in order to get rid of unwanted degrees of freedom. The resulting system of coupled PDEs is generally only solvable numerically, which means that in that case just the background (not accounting for conductivity or other responses) is computationally expensive and susceptible to errors.

We can engineer the relaxed RN action as an alternative to this difficulty by adding *linear axions* (massless scalar fields)

$$\Psi_x = \beta x,\ \Psi_y = \beta y \tag{2.16}$$

$$S_\Psi = -\int d^4x \sqrt{-g}((\partial\Psi_x)^2 + (\partial\Psi_y)^2) \tag{2.17}$$

$$S_{\mathrm{RN,rel}} = S_{\mathrm{EHM}} + S_\Psi \tag{2.18}$$

to our model, as has been done by Andrade and Withers [15] in the RN case and Kim et al. [16] for the holographic superconductor. Here, β dials the strength of translational symmetry breaking. The background solutions remain homogeneous, analytically solvable and reproduce the correct AC conductivity as we will show in the following. When including linear axions, the bulk stress tensor remains conserved, while the boundary stress tensor now includes dissipation of momentum [15].

The emblackening factor becomes

$$f(z) = (1-z)\left(1 + z + \frac{2-\beta^2}{2}z^2 - \frac{\mu^2 z^3}{4}\right) \tag{2.19}$$

by which the temperature decreases to

$$T_{RN\beta} = \frac{12 - \mu^2 - \beta^2}{16\pi}. \tag{2.20}$$

Therefore, also β/μ is dimensionless and we have next to T/μ and the horizon another physical scale that changes the state of our system. The equations of motion for Ψ_i just demand the second derivative to vanish and therefore Eq. (2.16) is a sufficient solution.

2.2.1 Results

Following the same steps towards the optical conductivity from the previous chapter while also perturbing the axions with small ψ_i

$$\Psi_i(x^i) \to \Psi_i(x^i) + \psi_i(z)e^{-i\omega t}, \tag{2.21}$$

the linearised equation of motion for a_y couples to the one for ψ such that (after eliminating the h_{ty}-component by using the right superposition of EOMs) we have

$$a_y''(z) - a_y'(z)\frac{f'(z)}{f(z)} + a_y(z)\left(\frac{z^2 f(z)A_t'(z)^2 - \omega^2}{f(z)^2}\right) - \frac{izA_t'(z)}{f(z)}\psi'(z) = 0 \tag{2.22}$$

$$\psi'''(z) + \psi''(z)\frac{f'(z)}{f(z)} + \psi'(z)\left(\frac{f'(z)f(z) - zf(z)\beta^2 + z\omega^2}{zf(z)^2}\right) - \frac{iz\beta^2 A_t'(z)}{f(z)}a_y(z) = 0. \tag{2.23}$$

	theoretical	fit $\beta = 0.1$	fit $\beta = 0$
ω_p^2	0.48	0.482	0.480
Γ	0.00476	0.00478	-
σ_Q	0.27	0.33	0.289

Table 2.1: Comparing theoretically expected values of plasmon frequency, momentum dissipation rate and universal conductivity to the measurement. *The theoretical values are obtained by combining Eqs.* (1.35), (1.38), (2.24) *and inserting the experimental parameters* $\mu = 3/2$ *and* $\beta\mu = 0.1$. *Fitting parameters are shown for both the translationally invariant* $\beta = 0$ *(Fig. 2.2 red) and the broken* $\beta = 0.1\mu$ *(Fig. 2.2 blue) system.*

Again, by solving these numerically, we obtain the optical conductivity shown in Figs. 2.4. In (a) and (b) we immediately recognise the expected Drude-like low-frequency behaviour from Fig. 1.1. By introducing the massless scalars Ψ_x, Ψ_y we therefore introduced momentum dissipation that increases with β. We see the redistribution of spectral weight from the δ-peak of Fig.1.1(a) to the Lorentzian of finite width. The Log-Log plot 2.4(c) shows the scale of the real part over all ω/μ. It becomes clear that the Drude part is well matched at low frequency, while the high frequency behaviour resembles the one of the zero density CFT. This combination looks like the trend that was measured for graphene [31]. Furthermore, 2.4(d) shows what the scaling of a divergence in the imaginary part (blue) looks like compared to a finite-width Lorentzian (red). We will later see that these two scalings can coexist in a non RN phase.

Together with this, there now is a finite DC conductivity that is – unlike σ_Q from Fig.2.3 – temperature independent. Fig.2.5 shows that in the case of broken translational symmetry, σ_{DC} depends only on the dimensionless parameter β/μ

$$\sigma_{DC} = 1 + (\beta/\mu)^{-2} \tag{2.24}$$

as found by Andrade and Withers [15]. We can use the relations of Eqs. (1.35), (1.38), (2.24) and the plasmon frequency

$$\omega_p^2 = \frac{\rho^2}{sT + \mu\rho} \tag{2.25}$$

to get a validation of our measurements, or more specifically, of the values of the fitting parameters ω_p^2, Γ, σ_Q. Table 2.1 shows that all fitting parameters reproduce the theoretically expected values quite well and therefore support our methods. Only σ_Q deviates slightly, as can also be seen in the $\omega/\mu \to 1$ asymptote between the two fits.

2.3 Interlude: Computation

Even the analytical part of computations can be massively simplified by using the right `Mathematica` packages that include covariant derivatives and internal calculation of the Riemann tensor and other GR variables. Especially the Einstein equations are significantly simplified and allow for playing around with different Ansätze for the metric. After double checking the equations of motion against the RN equations of [32] or the superconductor equations of [16], we continue to solving them.

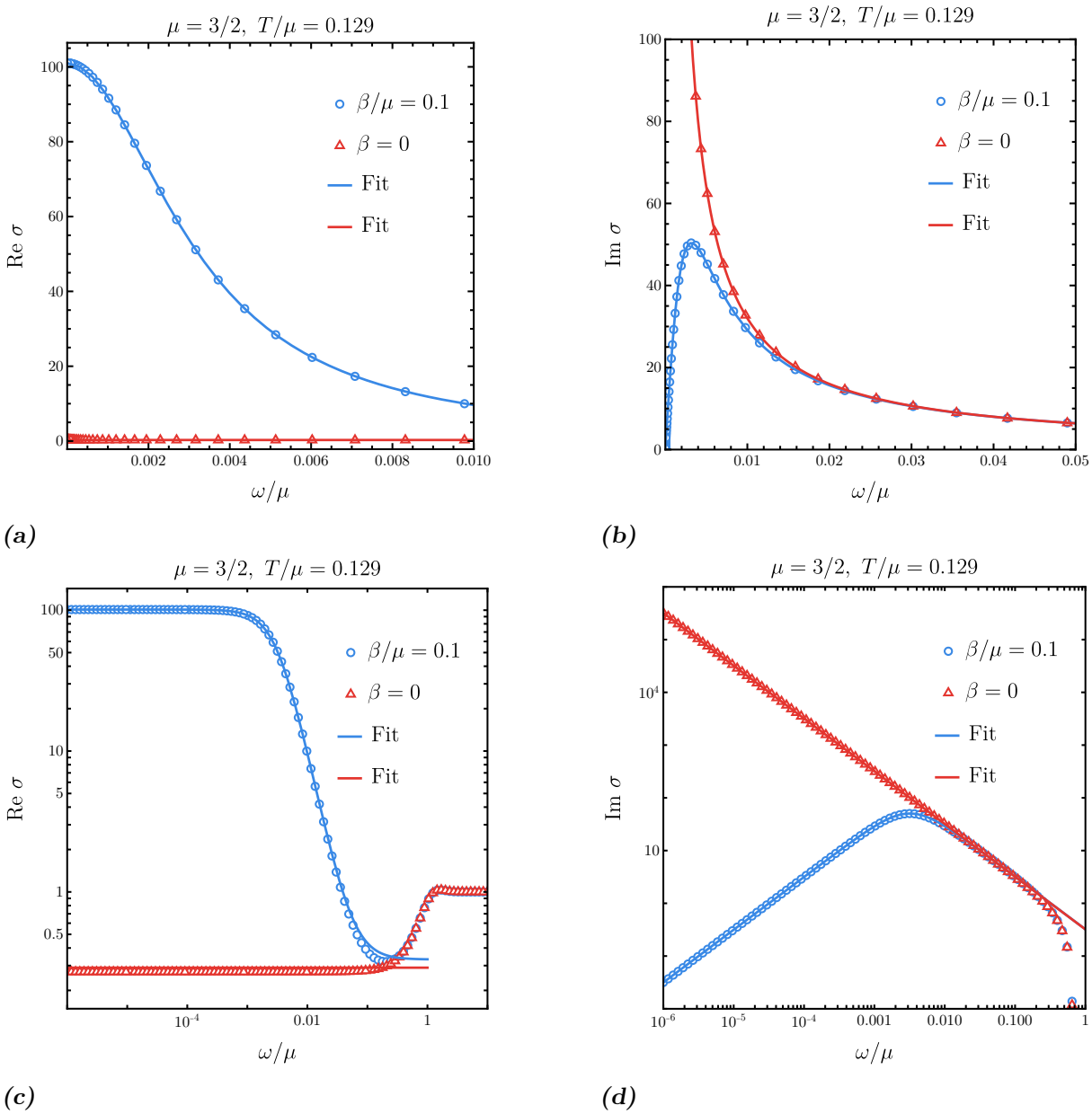

Figure 2.4: Drude-like conductivity in an RN metal. *The figures show the real (a), imaginary (b) part and the LogLog thereof (c),(d) of the optical conductivity. Previous results of the translationally invariant system $\beta = 0$ for comparison in blue and broken translational symmetry $\beta = \mu/10$ in red. Parameters for the blue curves fitted to Eqs. (1.36),(1.37): $\omega_p^2 = 0.48,\ \Gamma = 0.00287,\ \sigma_Q = 0.291$. Parameters for the red curves fitted to the non-δ parts of Eq. (2.14): $\omega_p^2 = 0.48,\ \sigma_Q = 0.269$. The discrepancy in the two σ_Q is visible in (c) by the repsective high frequency asymptote.*

Version of June 27, 2024– Created June 27, 2024 - 01:41

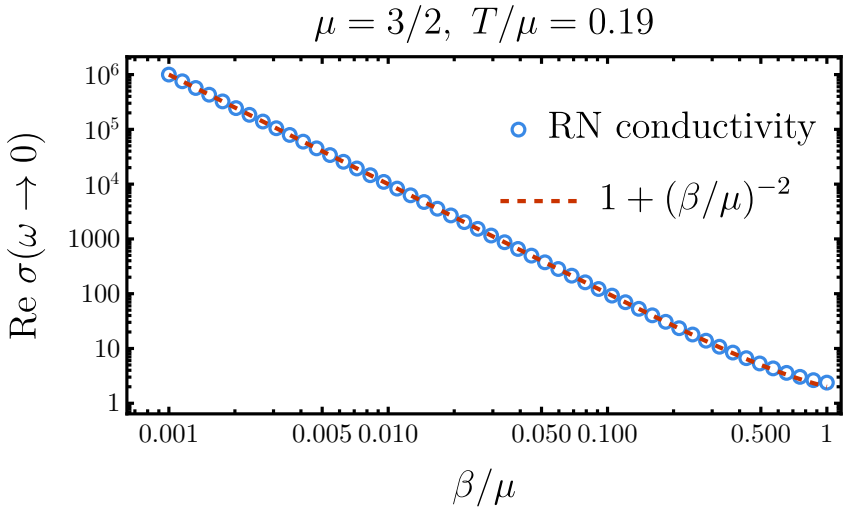

Figure 2.5: DC conductivity over translational symmetry breaking strength β/μ**.** *The real part of the optical conductivity for* $\omega \to 0$ *shows the* β/μ *dependence of Eq.* (2.24) *predicted by Andrade et al. [15], exhibiting temperature independence.*

In the case of a simple RN background with relaxation, where we know that closed solutions exist, one can solve Eqs. (1.17), (1.18) for the gauge potential $A_t(z)$ and the emblackening factor $f(z)$ with `DSolve` given the right boundary conditions

$$f(0) = 1\text{: asymptotically AdS} \qquad A(0) = 0\text{: regularity} \tag{2.26}$$

$$f(1) = 0\text{: vanish at horizon} \qquad A(1) = \mu\text{: source current.} \tag{2.27}$$

Via Eq. (1.15) we therefore also get $T_{RN\beta}$.

In the case of a more involved background (like the explicit lattice $\mu(x, y)$ or the superconductor ϕ, χ) and in the case for conductivities there are no closed analytical solutions anymore. In this case, we have to rely on `NDSolve` or other language's packages. Of course, the more computationally expensive systems are solved in `Python` or `C++`, as for example [14] did. For this work, `Mathematica` is sufficient.

Let us look precisely at how one can solve a system of (coupled) differential equations like Eqs. (2.9) or, more interestingly, (2.22) coupled to (2.23) using `Mathematica`. These are second order ordinary differential equations which need two initial conditions in order to be solved. We use the so-called shooting method [23, 32] where one boundary condition is enough to then guess, or *shoot for*, the second boundary condition.

The first boundary condition for each equation is *regularity at the horizon.* We express fields by their expansion in $z = 1$ as

$$a_y(z) = a_0 + a_1(1 - z) + a_2(1 - z)^2 + \cdots , \tag{2.28}$$

plug them into the equations of motion and demand that non-regular parts vanish. This way, all $a_{i>0}$ can be expressed in terms of a_0, such that a_0 remains as the variable for shooting. To give an example, for Eq. (2.9) this means (after replacing a_y with the in-falling boundary Ansatz of Eq. (2.13))

$$a_1 = -\frac{4(\mu^6 - 3i\mu^4(-8i + \omega) - 48\omega(3i + 2\omega) + 24\mu^2(6 + 2i\omega + \omega^2))}{((-12 + \mu^2)^2(-12 + \mu^2 + 8i\omega))} a_0 \tag{2.29}$$

The process can be repeated for higher orders to get more accuracy, i.e. to get $a_2 = a_2(a_0)$ and more.

For any guess now, $a_0 = 5$ for example, there is by Picard-Lindelöf one uniquely defined solution to the second order ODE in question. We find out whether it is the correct solution by solving with $a_0 = 5$ and $a_1 = a_1(a_0)$ and seeing whether the resulting $a_y(0)$ matches the boundary source we want it to hit. As a reminder, just as setting the boundary value of our background field $A_t(0) = \mu$, we need to source the fluctuation $a_y(0) = 1$ in the UV. A simple `FindRoot` will shoot for and find the *correct 5* that gives the right trend for $a_y(z)$. The solution can then be used to get a numerical value for the optical conductivity of Eq. (2.11), as `Mathematica` allows differentiation even of numerically interpolated functions.

This procedure can be followed for multiple coupled differential equations, as long as the boundary conditions obtained in this way are accurate enough such that shooting for a solution gives the expected result.

A more universal approach to solving these linearised equations of motion using gauge invariant modes and equations is presented in section 4.2.

2.4 A different approach to momentum dissipation

There is another way to account for dissipation of momentum that is conceptually more straight forward, physically more relevant, but computationally much more involved: a black hole lattice. The idea is to make the black hole background inhomogeneous by encoding an ionic lattice in the chemical potential. For the field theory, this corresponds to adding a modulated source to the Lagrangian [8], which gives room for a more physical interpretation of the source for momentum dissipation than the axion we used in the previous chapter. An example for this is a harmonic two dimensional potential of the form

$$\mu(x, y) = \mu_0 + \hat{A}_x \cos(k_x x) + \hat{A}_y \cos(k_y y), \tag{2.30}$$

where the strengths of the lattice $\hat{A}_x$, $\hat{A}_y$ are small and k_x, k_y are the wave vectors determining lattice spacing. Respecting the boundary condition that

$$A_t(z \to 0) = \mu(x, y), \tag{2.31}$$

there no longer exists a closed solution for A_t. This way, the translational symmetry in x- and y-direction is broken and therefore the background fields now depend on the holographic *and* spatial dimensions. In the Reissner-Nordström case we consider the spacetime Ansatz of [14], that was in turn adapted from [33]

$$\begin{aligned} ds^2 &= \frac{1}{z^2}\left(-Q_{tt} f(z)\eta_t^2 + Q_{xx}\eta_x^2 + Q_{yy}\eta_y^2 + \frac{Q_{zz}}{f(z)\eta_z^2}\right) \\ \eta_t &= dt \\ \eta_x &= dx + Q_{xy}dy + Q_{xz}dz \\ \eta_y &= dy + Q_{yz}dz \\ \eta_z &= dz \end{aligned} \tag{2.32}$$

to account for the backreaction of the lattice on the metric. Here we introduced the tetrad formalism accounting for the coupling of various spatially dependend modes. The functions $Q_{\mu\nu} = Q_{\mu\nu}(x, y, z)$ are periodic in (x, y) and a priori only constrained by the symmetry requirement of the metric, that is, introducing 10 new degrees of freedom. This makes Eqs. (1.17),(1.18) into 3 dimensional partial differential equations. Solutions to this were calculated by Balm et al. [14] for the RN and the Einstein-Maxwell-Dilaton system. The problem with getting the optical conductivity in y-direction now is not only that many more modes instead of just g_{ty} (see discussion around Eq. (2.9)) couple to a_y, but also that one needs to fix all the remaining degrees of freedom by choosing the right boundary conditions in order to solve the PDEs. The requirement for Eq. (2.32) to be asymptotically AdS gives some boundary conditions in the UV, while regularity constraints the IR.

An approach to reduce unwanted background degrees of freedom related to the search for gauge independent variables presented in section 4.2, is the DeTurck method. This is based on modifying the Einstein tensor by the DeTurck vector that depends on a simpler reference metric as shown in [6, 12]. For the conductivity we can then go into Lorenz and De Donder gauge[10].

Following all this, we applied the same logic of finding boundary conditions constraining the near-horizon behaviour of $f(z)$ and the $Q_{\mu\nu}(x, y, z)$ by demanding regularity. `Mathematica` is of great help when it comes to expanding to a certain order and getting constraints on leading orders. At a certain point, however, when the equations of motion become even more untractable and one also wants to include for perturbations to eventually also describe the conductivity, the naive and straight forward approach we took did not yield the results we hoped. The next step here would be to get all final equations and the right amount of boundary conditions constraining the system and finally solve it using the software package developed by Balm et al. [14] written in `C` and `Python` running on a cluster. This was not the direction we chose to go and rather stuck with using the linear axion model to account for momentum dissipation. This way, we kept the computations smaller and handable inside of `Mathematica` on a personal computer.

Version of June 27, 2024– Created June 27, 2024 - 01:41

Chapter 3

Holographic Superconductor

The proposal of the holographic version of a superconductor in 2008 by Hartnoll, Herzog and Horowitz [5] sparked some new hope in the validity and applicability of holography to condensed matter systems. The so called HHH model is considered a superconductor, or more precisely, a super*fluid* in the most fundamental way, that a global $U(1)$ is spontaneously broken in the boundary field theory. They found a way to trigger an instability that would break the local $U(1)$ of the bulk in the infrared while keeping the UV symmetry intact. By the global-local symmetry stated in GKPW, we see that the break down of the local $U(1)$ must be immediately connected to that of the global one. More precisely, the field triggering the instability in the bulk is be dual to the boundary operator whose vacuum expectation value (VEV) can be seen as the order parameter of the superfluid phase transition. In this way, they managed to spontaneously create an asymmetric VEV in the boundary without explicitly sourcing the operator.

The holographic superconductor has been studied in the probe limit [5], including backreaction on the background [34], under translational symmetry breaking using linear axions [16], [35], in the zero temperature limit [36], as a *bona fide* superconductor [37] (not just a superfluid) and many more. We gain insights from each direction of research but will introduce the holographic superconductor not as the main subject of our study, rather as another building block of our RN system. We introduce the superfluid in order to augment the field theory by its characteristic low-energy excitations. More specifically, with breaking the global $U(1)$ comes an additional Goldstone mode [37] that we hope will mimic the role of phonons in a real strongly interacting metal. Before we test the effect of this, however, we should lay some theoretical and numerical groundwork and understand how the Holographic Superconductor by itself works. Only after we have done this will we look at its effect on our relaxed RN model.

3.1 Preliminaries

Let us look at how a RN to superconductor phase transition is engineered in a gauge-gravity dual system. In section 1.2.3 we already looked at the mass-scaling duality in Eq. (1.32) of a scalar bulk field. From there we can see that something funny happens for

$$m^2 < -\frac{(d+1)^2}{4} = -\frac{9}{4}, \tag{3.1}$$

where again d counts the number of spatial dimensions that are not holographic ($d = 2$ for us). Eq. (3.1) is known as the Breitenlohner-Friedman bound [38] beyond which AdS space becomes unstable. Therefore, the mass squared can be negative, but not more negative than the BF bound. The near-horizon geometry of our AdS space with RN black hole, however, looks different. As we have mentioned before, the most interesting deviations from pure AdS/CFT happen close to the horizon at $z = 1$. When expanding the metric, we see [9] that the geometry actually resembles $\mathrm{AdS}_2 \times \mathbb{R}^2$ instead of AdS_4, having the result that the BF bound of Eq. (3.1) increases to $-1/4$ at the horizon. For O to be a relevant operator, $\Delta < d + 1$ and therefore $m^2 < 0$, which together with the raised BF bound close to the IR becomes quite the narrow window. Furthermore, the term in Eq. (3.6) proportional to $A_\mu A^\mu = g^{tt} A_t^2$ further decreases m, or rather raises the BF bound by some b. This means that a field of mass

$$-\frac{9}{4} < m^2 < -\frac{1}{4} + b \tag{3.2}$$

triggers an instability in the IR but not the UV. When the instability is triggered, we say that ϕ condenses. One can think of the scalar field as a cloud of charged particles surrounding the black hole, in balance between being repelled by the charge of the black hole and the potential barrier naturally given by AdS space. A more rigorous picture is painted by [9] in chapter 10.

3.2 The setup

We start off with the relaxed RN action in Eq. (2.18) from before and couple a scalar field ϕ to the $U(1)$-gauge potential A_μ, such that the former triggers a Higgs mechanism [9], [37] in the deep IR. This way, the action and equations of motion become

$$S_{\mathrm{HHH,rel}} = S_{\mathrm{RN,rel}} - \int d^4x \sqrt{-g} \left(|(\partial_\mu - iqA_\mu)\phi|^2 + m^2|\phi|^2 \right) \tag{3.3}$$

and

$$R_{\mu\nu} - \frac{1}{2} R g_{\mu\nu} - 3 g_{\mu\nu} = \frac{\kappa^2}{2} (T^{\mathrm{Max}}_{\mu\nu} + T^{\Psi}_{\mu\nu} + T^{\phi}_{\mu\nu}) \tag{3.4}$$

$$\nabla_\mu F^{\mu\nu} = -iq \Big[\phi^* (\partial^\nu - iqA^\nu)\phi - \phi(\partial^\nu + iqA^\nu)\phi^* \Big] \tag{3.5}$$

$$(\nabla^\mu - iqA^\mu)(\nabla_\mu - iqA_\mu)\phi - m^2\phi = 0, \tag{3.6}$$

respectively. By introducing this, a lot has changed in the way we can solve the dynamics for this system. Where the solutions to our previous systems were analytically available, we do not know of a closed solution to Eqs. (3.4)-(3.6). We do know that the Ansatz for the background metric has to be changed in order to allow for deformations in the IR to

$$ds^2 = \frac{1}{z^2} \Big[-f(z) e^{-\chi(z)} dt^2 + \frac{dz^2}{f(z)} + dx_i dx^i \Big]. \tag{3.7}$$

For $\phi, \chi \to 0$ the RN equations of motion and their solutions are recovered. We assume $\phi = \phi(r)$ to depend only on the holographic dimension. With this we can deduce from the z-component of Eq. (3.5) that ϕ has a constant phase and can therefore be chosen to be real. This will change when considering perturbations in the scalar field around the background solution. Expanding the metric at the horizon, we find the temperature of the holographic superconductor as

$$T_{SC} = e^{-\frac{\chi(1)}{2}}\left(12 - 2\beta^2 + 4\phi(1)^2 - e^{\chi(1)}A_t'(1)^2\right)\frac{1}{16\pi}, \tag{3.8}$$

where all fields are evaluated at the horizon $z = 1$. The temperature agrees with [34]. Due to f, χ, it can only be calculated numerically. In the following, we always choose the mass of the scalar field as $m^2 = -2$, that is, a naive scaling dimension of Eq. (1.32) $\Delta = 2$ for the dual operator O. We rescale by to get the desired UV leading and sub-leading order behaviour

$$\phi/z = \tilde{\phi} \sim A + Bz, \tag{3.9}$$

such that

$$\tilde{\phi}(0) = A = J_O \text{ and } \tilde{\phi}'(0) = B = \langle O \rangle, \tag{3.10}$$

where in the last equalities we have used the dictionary translation of (sub-)leading bulk field behaviour in the UV to (response) source of the dual operator O. We will see that $\langle O \rangle$ is the order parameter of the superfluid phase transition in the boundary theory. The idea is to tune ϕ such that the sub-leading order B spontaneously becomes non-zero, while the leading order stays zero throughout. A non-zero leading order would imply explicit sourcing of O and therefore explicit and not spontaneous symmetry breaking. To get explicit values, we need to solve the coupled differential equations Eqs. (3.4)-(3.6).

3.3 Superconducting phase transition

The same procedure we followed in section 2.3 for numerically solving for the optical conductivity can now be applied to finding *background* solutions, as both just boil down to solving coupled differential equations. Remember that the background was analytical up until here, making all following computations that include $\phi, \chi \neq 0$ much more involved and computationally expensive. From here on out, therefore, we will work with background functions f, χ, A_t, ϕ in the form of functions interpolated by `Mathematica`. These solutions are shown at $T/\mu = 0.144$ below the critical temperature $0.157 = T_c/\mu$ in Fig. 3.1.

Figs. 3.2 show the ratio of the background fields of the SC solution relative to the RN solution. More specifically, Fig. 3.2(a) confirms that the numerics work, that is, above the condensation temperature numerics and analytical solution agree. In Fig. 3.2(b) we see how below the critical temperature, the scalar field becomes non-zero in the IR and backreacts on the all other fields. Asymptotically, both solutions still agree and the ratio is 1. The only exception being A_t, as μ has to be tuned differently in the RN phase to get the backgrounds at the same temperature.

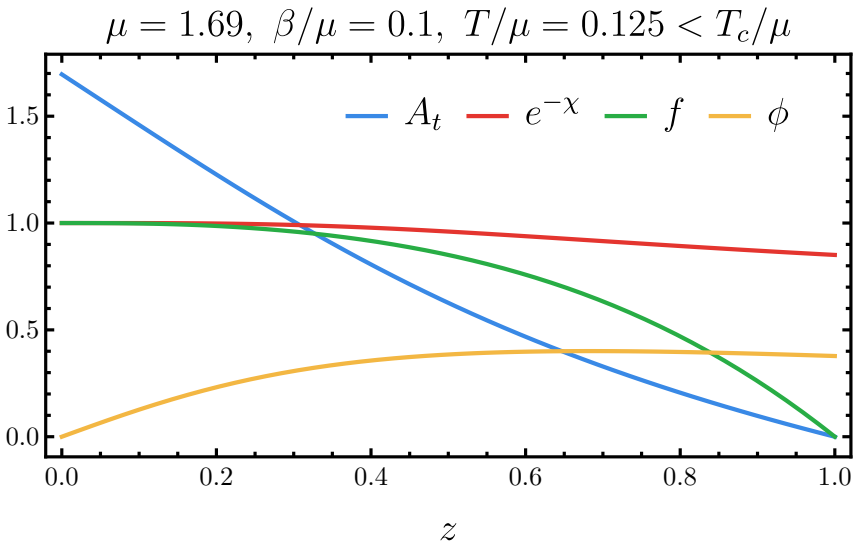

Figure 3.1: Numerical solution for the bulk fields of the holographic superconductor. *Below the critical temperature of $T_c/\mu = 0.157$, there is a clear condensation of the scalar field ϕ in the IR. The fields asymptotically agree with the RN solution in the UV and start to deform for $z \to 0$.*

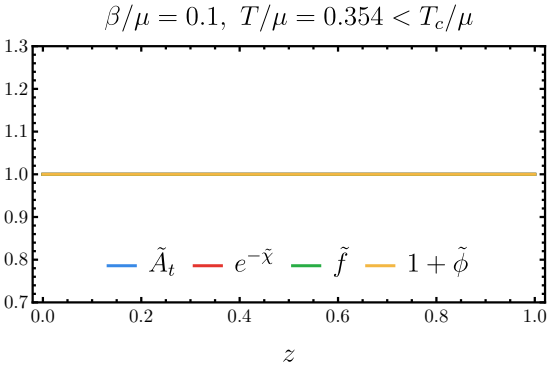

(a) *Above condensation at $T/\mu = 0.354 > T_c$, numerical and analytical solution are identical. All field ratios are superposed at 1.*

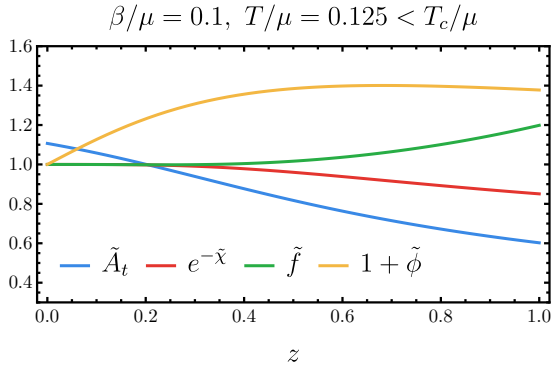

(b) *Below condensation at $T/\mu = 0.1444 < T_c$, ϕ immediately backreacts on the entire background and the numerical solution becomes different to the analytical background everywhere $z > 0$. The slight deviation of $\tilde{A}_t(0) \neq 1$ stems from $\mu_{RN} \neq \mu_{SC}$, see also Fig.3.3(b).*

Figure 3.2: Ratio of numerical to analytical background solutions above and below $\mathbf{T_c}$. *Fields with tilde represent the respective ratio numerical/analytical solution for the holographic dimension z going from the UV to the horizon: $\tilde{A}_t = A_t^{SC}/A_t^{RN}$. A constant was added to ϕ to avoid division by zero in the RN phase.*

In Fig. 3.3(a) we see the second order phase transition for the response of the field operator O dual to ϕ, while the source stays zero throughout: We have succeeded in replicating the HHH model of a holographic superconductor. Fig. 3.3(b) shows, that the condensation – ϕ becomes non-vanishing – increases the field theory temperature, agreeing with Eq. (3.8). It shows, that when comparing the two different phases RN and SC, we need to tune the chemical potential of one in order to guarantee a constant physical temperature T/μ. This will become important in the next chapter where we want to measure the impact of the superconducting state on the coexisting normal state.

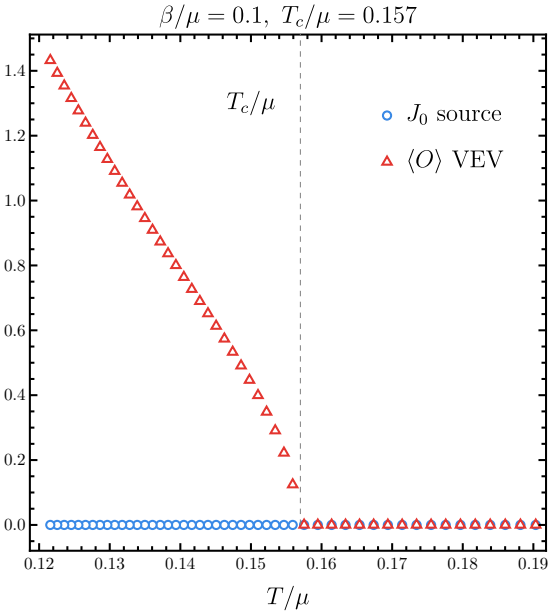

(a) *Phase transition of $\langle O \rangle$ without explicitly sourcing O. The critical temperature in units of the chemical potential is $T_c/\mu = 0.157$. The other physical parameter $\beta/\mu = 0.1$ is kept constant. We are considering standard quantisation, where $m^2 = -2$ and $q = 3$.*

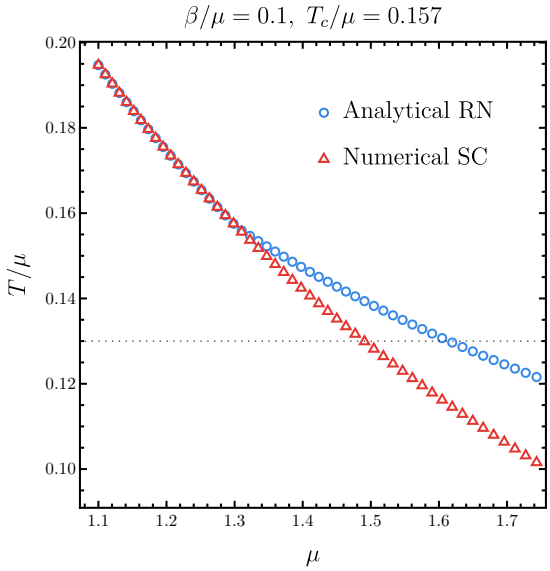

(b) *Temperature T/μ over chemical potential μ in the SC phase (red) deviates from the analytical RN temperature (blue). In concordance with Eqs. (3.8), the condensed ϕ increases the temperature. To be able to compare an SC to RN system, one must look some constant physical temperature T/μ, i.e. at different chemical potential following the dotted line.*

Figure 3.3: Spontaneous symmetry breaking of the SC order parameter and the change in temperature at phase transition. *The phase transition is observed for varying chemical potential μ (directly related to the temperature) and keeping $\beta/\mu = 0.1$ fixed.*

3.4 Conductivity of the relaxed Holographic Superconductor

On top of the numerical background solution to the equations of motion, we can again look at the linear response of the system. Next to the perturbations of the gauge potential Eqs. (2.7), the metric (2.8) and the axions (2.21), we also consider

$$\phi \to \phi(z) + \delta\phi(z) e^{-i\omega t}. \tag{3.11}$$

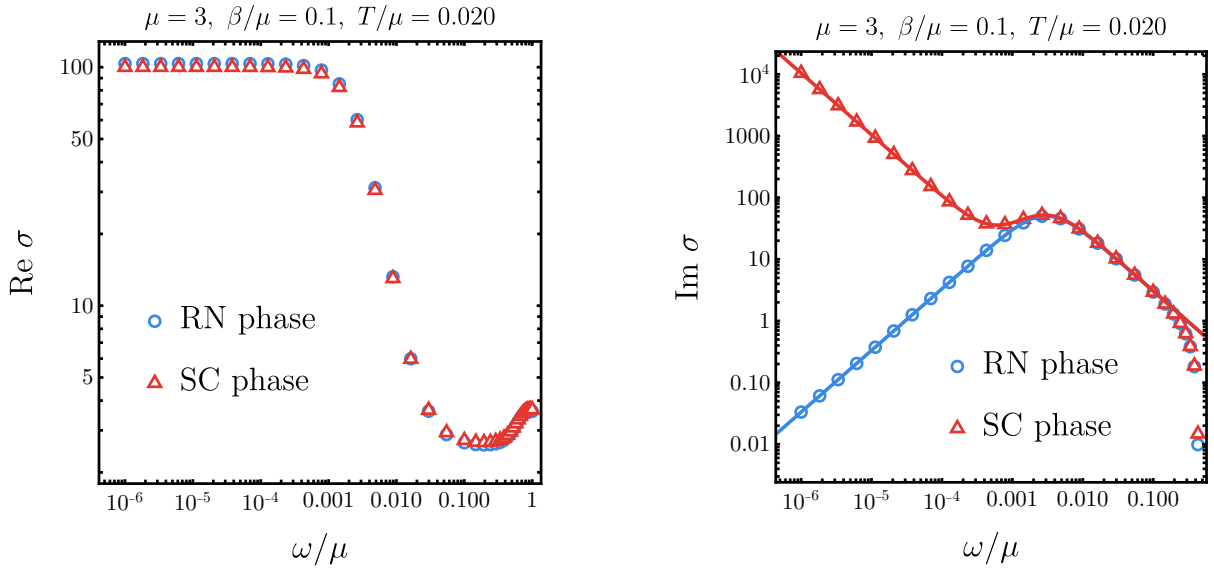

(a) ***(b)***

Figure 3.4: Conductivity of the relaxed holographic superconductor. *(a) Real and (b) imaginary part of the conductivity over the frequency ω/μ. The normal RN phase (blue) in comparison to the condensed SC phase (red). The data is fitted to Eq. (3.13) with values for SC: $\sigma_0 = 97,\ \Gamma = 0.003,\ \sigma_s = -0.01$ and RN: $\sigma_0 = 101,\ \Gamma = 0.003,\ \sigma_s = 10^{-10}$. At high ω/μ both conductivities approach the zero density CFT description and diverge from the Drude model.*

In this case (no momentum dependence), the fluctuation in ϕ decouples from $a_y(z)$ and the dynamics of $a_y(z)$ in Eq. (2.22) are only changed with respect to the previous chapter by the different background solution where $\phi, \chi \neq 0$. From here, it would be an interesting investigation to vary the phase of the fluctuation $\delta\phi$ and see how its dynamics couple in the finite k sector.

Comparing the conductivity on the analytical RN background with the conductivity on the numerical SC background at the same temperature T/μ, we observe that the latter can be described as a two fluid system

$$\sigma_{\text{2FL}}(\omega) = \frac{\sigma_0\,\Gamma}{\Gamma - i\omega} + \frac{\sigma_s}{i\omega} \tag{3.12}$$

$$\text{Im}\,\sigma_{\text{2FL}}(\omega) = \frac{\sigma_0\,\Gamma^2}{\Gamma^2 + \omega^2} - \frac{\sigma_s}{\omega}, \tag{3.13}$$

$$\tag{3.14}$$

as was also observed by Kim et al. [16] and Andrade et al. [35]. The conductivity shows that just as in condensed matter superfluid systems, parts of the fluid remain normal while others are superfluid. In Fig. 3.4, we see this as the superposition of a δ-peak with the finite-width Lorentzian, one describing perfect conductivity and the other a normal metal, respectively. Looking more closely at the DC-behaviour of σ in Fig. 3.5 at $\beta = 0$, we see that the real part in fact does decrease with condensation, while the imaginary part increases. The loss in spectral density is compensated by the increase of the imaginary part. Combining the translationally invariant conductivity Eq. (2.14) with the two fluid

model gives

$$\sigma(\omega) = (K_s + K_n)\left(\delta(\omega) - \frac{1}{i\omega}\right), \tag{3.15}$$

with K_n, K_s the strength of the respective normal and superfluid part of the δ. Taking that the spectral weight must be conserved [16] for some constant $Z(\Lambda \to \infty)$ we have

$$Z(\Lambda) = \int_0^\Lambda \mathrm{Re}\,\sigma(\omega)d\omega = K_s + K_n + \sigma_Q\Lambda \tag{3.16}$$

$$\Leftrightarrow \mathrm{Re}\,\sigma(\omega) = \frac{Z(\Lambda) - K_n - K_s}{\Lambda} \tag{3.17}$$

while

$$\mathrm{Im}\,\sigma(\omega) = \frac{K_n + K_s}{\omega}. \tag{3.18}$$

Therefore, going from RN to SC, that is, $K_s = 0 \to K_s > 0$, means that the real part *decreases* and the imaginary part *increases*, confirming our observations from Fig. 3.5.

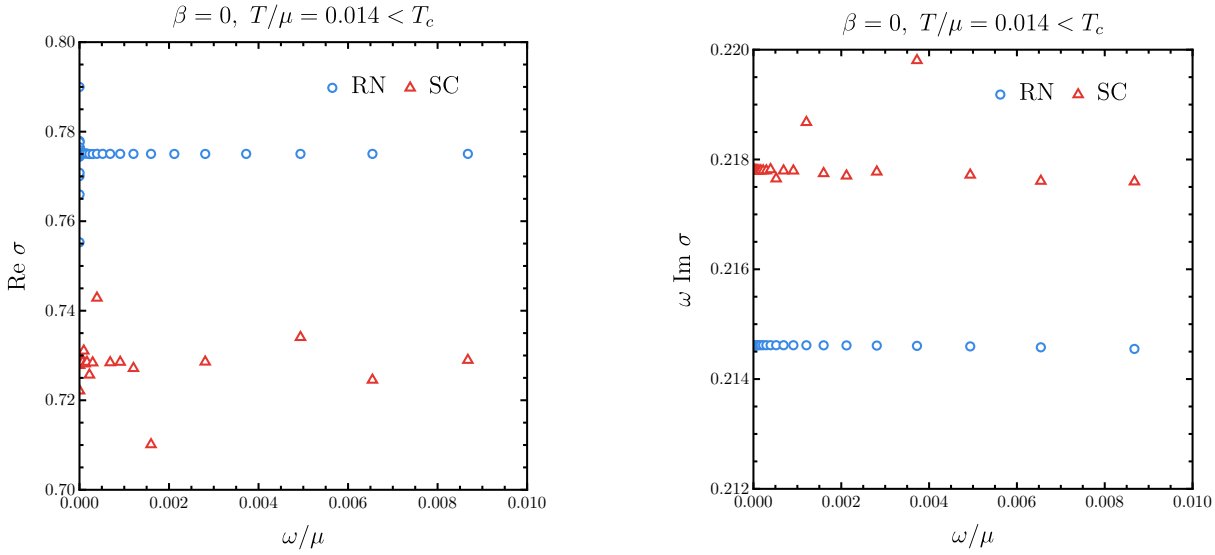

(a) ***(b)***

Figure 3.5: Change of spectral weight from RN to SC phase at $\beta = 0$. *Low frequency $\omega/\mu \ll 1$ asymptote of (a) $\mathrm{Re}\,\sigma$ and (b) $\omega\,\mathrm{Im}\,\sigma$. The real part shows a drop in DC conductivity, indicating a loss of spectral density that is compensated by the increase in the imaginary part. The imaginary part is multiplied by ω to counter the divergence and therefore to better compare the respective DC behaviour. Here, the translationally invariant system at $\beta = 0$ is considered and both solutions are obtained at the same T/μ below T_c/μ. The SC conductivity being based on a numerical background is more unstable than the RN conductivity on the analytical background.*

Following, one could further investigate properties of the holographic superconductor, like the dependence of T_c on the charge q [34], the phase transition at different strengths of translational symmetry breaking β [16] and conductivity [35]. As mentioned before, we will only use the superconductor as a means to introduce new modes our charge carriers

can interact with and not to test properties of the superconductor itself. Therefore, we are not really interested in the two fluid itself, but the effect it will bring onto another charge we add to the system. Let us now go into realms that have not been tested before and consider the impact of adding a holographic superconductor on top of an RN metal, such that the system consists of said two $U(1)$-charges.

Chapter 4

The Two Charge Holographic Superconductor

We are now in a position to combine the approaches of the previous two chapters to get the Two-Charge Holographic Superconductor. One charge A_μ, associated with the Reissner-Nordström phase, being the one under investigation and another one B_μ that comes coupled to a scalar field ϕ constituting the holographic superconductor. We will call the normal phase RN2 and the superconducting SC2 to not confuse them with the previous system's phases.

4.1 The Set Up

By now we know how to add to our system to get the expected field theory behaviour. The full action we are considering is therefore the sum of all the previous ones

$$\begin{aligned} S = \frac{1}{2\kappa^2}\int d^4x\,\sqrt{-g}\Bigg[R + 6 - \frac{1}{4}F_{\mu\nu}F^{\mu\nu} - \frac{1}{4}W_{\mu\nu}W^{\mu\nu} \\ -\frac{1}{2}\sum_{i=x,y}(\partial\Psi_i)^2 - |(\partial_\mu - iqB_\mu)\phi|^2 - m^2|\phi|^2\Bigg], \end{aligned} \tag{4.1}$$

where $F = dA$, $W = dB$ and again $2\kappa^2 = 16\pi G = 1$. The equations of motion are

$$R_{\mu\nu} - \frac{1}{2}Rg_{\mu\nu} - 3g_{\mu\nu} = \frac{\kappa^2}{2}\left(T^{\text{Max},A}_{\mu\nu} + T^{\text{Max},B}_{\mu\nu} + T^{\Psi}_{\mu\nu} + T^{\phi}_{\mu\nu}\right) \tag{4.2}$$

$$\nabla_\mu F^{\mu\nu} = 0 \tag{4.3}$$

$$\nabla_\mu W^{\mu\nu} = iq\Big[\phi^*(\partial^\nu - iqA^\nu)\phi - \phi(\partial^\nu + iqA^\nu)\phi^*\Big] \tag{4.4}$$

$$(\nabla^\mu - iqA^\mu)(\nabla_\mu - iqA_\mu)\phi = m^2\phi. \tag{4.5}$$

One has to pay attention to the renaming, as now B_μ is coupled to ϕ and A_μ has the same role it had in chapter 2. Above the critical temperature, therefore we have a system of equivalent RN1 setups, together RN2. Below the critical temperature, ϕ again triggers an instability of AdS close to the horizon, such that the gauge $U(1)$ associated with B_μ is broken and therefore also the global $U(1)$ associated with O_B dual to B_μ. The phase

below T_c is therefore made up of RN1 plus holographic superconductor and we call it SC2 – keeping in mind that only one of the two metals can transition into a superconducting state.

Looking close to the horizon, we find the temperature

$$T_{SC2} = e^{-\frac{\chi(1)}{2}}\left(12 - 2\beta^2 + 4\phi(1)^2 - e^{\chi(1)}\left(A_t'(1)^2 + B_t'(1)^2\right)\right)\frac{1}{16\pi}, \tag{4.6}$$

which reduces to Eq. (3.8) for $B_t = 0$. It also recovers the RN2 temperature for $\chi = \phi = 0$ and $A_t(z) = \mu_A(1-z), B_t(z) = \mu_B(1-z)$ where

$$T_{RN2} = \frac{|f'(1)|}{4\pi} = \frac{12 - (2\beta^2 + \mu_A^2 + \mu_B^2)}{16\pi}, \tag{4.7}$$

from the emblackening factor

$$f(z) = (1-z)\left(1 + z + \frac{2-\beta^2}{2}z^2 - \frac{\mu_A^2 + \mu_B^2}{4}z^3\right). \tag{4.8}$$

4.2 Interlude: Gauge invariant modes

Having introduced all the fields of our system, let us find a more universal way to solve for the dynamics of their their time dependent perturbations

$$\begin{aligned} g_{\mu\nu} + h_{\mu\nu}(z)e^{-i\omega t}, \quad & A_\mu + a_\mu(z)e^{-i\omega t}, \quad & B_\mu + b_\mu(z)e^{-i\omega t}, \\ \phi + \varphi(z)e^{-i\omega t}, \quad & \Psi_x + \psi_x(z)e^{-i\omega t}, \quad & \Psi_y + \psi_y(z)e^{-i\omega t}, \end{aligned} \tag{4.9}$$

where $||h_{\mu\nu}|| \ll ||g_{\mu\nu}||$ and so on. We collectively call the lower case fields $\pi_i(z)$. Now, instead of manually choosing – as for $a_y(z)$ in Eq. (2.9) – which modes are of interest, we can zoom out a bit and rely on first principles: the physics cannot be *gauged away* and will therefore be described by *gauge invariant* variables and equations. There are certain superpositions of our perturbations and their equations of motion that are gauge invariant. Finding these superpositions reduces the number of coupled differential equations and the fields we have to solve for drastically. Furthermore, the resulting modes are more comparable to other's work, because we can all agree on first principles. They will also allow for a more physical interpretation of the modes we are looking at. We will see that, for example, the fields $a_y,\ b_y$ remain gauge invariant, underlining their physical relevance and ensuring that we don't have to consider other conductivities.

For the fields π_i to be invariant under simultaneous coordinate transformation (diffeomorphism invariance) of the metric and gauge invariance of the gauge potentials, they must be invariant under

$$\begin{aligned} h_{\mu\nu} &\to h_{\mu\nu} - \nabla_\mu\xi_\nu - \nabla_\nu\xi_\mu \\ b_\mu,\ a_\mu &\to a_\mu - \partial_\mu\lambda^{(a)} - \xi^\gamma\nabla_\gamma a_\mu - a_\gamma\nabla_\mu\xi^\gamma \\ \psi_x,\ \psi_y,\ \varphi &\to \varphi - \xi^\gamma\partial_\gamma\varphi \\ \xi^\mu(z,t) &= \tilde{\xi}^\mu(z)e^{-i\omega t} \\ \lambda^{(a,b)}(z,t) &= \tilde{\lambda}^{(a,b)}(z)e^{-i\omega t} \end{aligned} \tag{4.10}$$

with the diffeomorphism $|\xi^\mu(z,t)| \ll 1$ and scalar fields $\left|\lambda^{(a,b)}(z,t)\right| \ll 1$. We follow the procedure laid out in [39] in order to find combinations of π_i for which $\xi,\ \lambda$ vanish.

To do this, we look at decoupling sectors, classified by their behaviour under parity inversion $y \to -y$ in our AdS_{2+2} system. The so-called *spin 0* sector stays invariant and the *spin 1* flips sign. Simply put: we separate such that perturbations that appear in the spin 0 sector have an even amount of y-indices and the ones in spin 1 an odd amount. Without a momentum term $\sim e^{ikx}$ in Eq. (4.9), the terms will further decouple but it is not as straight forward as with the sectors to see how. The 21 fields split into sectors as

$$\text{Spin 0} \qquad a_t, a_x, a_z, b_t, b_x, b_z, \varphi, \psi_x, h_{tt}, h_{tx}, h_{tz}, h_{xx}, h_{xz}, h_{yy}, h_{zz} : 15 \tag{4.11}$$

$$\text{Spin 1} \qquad a_y, b_y, \psi_y, h_{ty}, h_{xy}, h_{yz} : 6. \tag{4.12}$$

The 6 components of $\{\xi^\mu, \lambda^{(a)}, \lambda^{(b)}\}$ together with the z-gauge where all z components vanish, we get $21 - 6 - 6 = 9$ degrees of freedom. Of these, 5 go into the spin 0 and 4 into the spin 1 sector.

We first consider the spin 1 sector, that is, where only Eq. (4.12) can couple to one another. To get the gauge invariant variable

$$\Gamma = \sum_{i=1}^{6} \alpha_i \pi_i, \tag{4.13}$$

we need to find α_i such that for $\Gamma \xrightarrow{(4.10)} \Gamma'(\xi^t, \xi^x, \xi^z, \lambda^{(a)}, \lambda^{(b)})$ we have

$$\Gamma' - \Gamma = \sum_{i=1}^{6} \alpha_i \Big(\pi_i'(\xi^\mu, \lambda^{(a,b)}) - \pi_i \Big) = 0. \tag{4.14}$$

In other words: Γ needs to be independent of $\{\xi^t, \xi^x, \xi^z, \lambda^{(a)}, \lambda^{(b)}\}$. Choosing gauges this way still does not fully fix our system and one can express the 6 α_i's by 4 free variables. We get the following four gauge independent variables in the spin 1 sector:

$$\left\{ \mathcal{A} = a_y,\ \mathcal{B} = b_y,\ \mathcal{C} = h_{xy},\ \mathcal{D} = h_{ty} + \frac{i\omega}{\beta}\psi_y \right\}, \tag{4.15}$$

where we have already rescaled such that the leading order is constant on the boundary, that is,

$$\mathcal{A}(z \to 0) = \mathcal{A}^{(0)} + \mathcal{A}^{(1)} z + \dots \tag{4.16}$$

$$\mathcal{B}(z \to 0) = \mathcal{B}^{(0)} + \mathcal{B}^{(1)} z + \dots \tag{4.17}$$

$$\mathcal{C}(z \to 0) = \mathcal{C}^{(0)} + \mathcal{C}^{(1)} z^3 + \dots \tag{4.18}$$

$$\mathcal{D}(z \to 0) = \mathcal{D}^{(0)} + \mathcal{D}^{(1)} z^3 + \dots, \tag{4.19}$$

$$\tag{4.20}$$

where the ellipses denote higher order terms. Following the GKPW dictionary, this means for example, that the boundary two-point correlator dual to $\mathcal{C}$ is easily obtained via

$$\langle O_{\mathcal{C}} O_{\mathcal{C}} \rangle \sim \left. \frac{\mathcal{C}'''(z)}{\mathcal{C}(z)} \right|_{z=0}. \tag{4.21}$$

For our purposes, we therefore express the conductivity with respect to the A gauge potential Eq. (2.11) in terms of $\mathcal{A}$ as

$$\sigma_A(\omega) = -\frac{i}{\omega}\frac{\mathcal{A}'(z=0)}{\mathcal{A}(z=0)} \tag{4.22}$$

One can re-state the equations of motion depending only on the background and the gauge invariant variables. The equations are reduced to the number of degrees of freedom: 4. The dynamics of $a_y(z)$ – now $\mathcal{A}(z)$ – are described by

$$\begin{aligned} 0 = \mathcal{A}'' + \mathcal{A}' \frac{-12 + 2z^2\beta^2 + 12f - 4z^2\phi^2 + e^{\chi}z^4(A_t')^2 + e^{\chi}z^4(B_t')^2}{4zf} \\ + \mathcal{A}\frac{e^{\chi}\omega^2\left(e^{\chi}\omega^2 - f\left(\beta^2 + e^{\chi}z^2(A_t')^2\right)\right)}{f^2\left(e^{\chi}\omega^2 - \beta^2 f\right)} - \mathcal{B}\frac{e^{2\chi}z^2\omega^2 A_t' B_t'}{e^{\chi}\omega^2 f - \beta^2 f^2} - \mathcal{D}'\frac{e^{\chi}\beta^2 A_t'}{e^{\chi}\omega^2 - \beta^2 f}, \end{aligned} \tag{4.23}$$

and of course the other gauge invariant's equations (see Appendix A). We see that $\mathcal{C}$ completely decouples and can restrict our investigation to $\mathcal{A}$, $\mathcal{B}$, $\mathcal{D}$ and their equations. It becomes clear immediately, that at finite k this would become vastly more complicated.

As opposed to the process of numerically solving the EOMs in `Mathematica` as described in section 2.3, we later solved them using a finite-differences method. After numerically solving the gauge invariant equations of motion for $\mathcal{A}$, $\mathcal{B}$, $\mathcal{D}$ in the general case $\chi, \phi \neq 0$ and not forgetting about the infalling boundary conditions, we can observe that the main properties of the previous chapters persist.

4.3 RN2 conductivity

With adding a second gauge potential to the system, we have to choose which potential to source and which conductivity to measure. When solving the linearised equations of motion, we either set

$$\mathcal{A}(0) = 1,\ \mathcal{B}(0) = 0 \text{ or } \mathcal{A}(0) = 0,\ \mathcal{B}(0) = 1, \tag{4.24}$$

and respectively measure either

$$\sigma_A(\omega) = -\frac{i}{\omega}\frac{\mathcal{A}'(z=0)}{\mathcal{A}(z=0)} \text{ or } \sigma_B(\omega) = -\frac{i}{\omega}\frac{\mathcal{B}'(z=0)}{\mathcal{B}(z=0)}. \tag{4.25}$$

In the following we have to be careful which conductivity we are talking about, because they play crucially different roles when in different phases. In general, we will refer to σ_A as the conductivity of interest, because, as we stressed, the superconductor is only a building block added on top of the RN system of interest. In Fig. 4.1 we show that in the non-condensed phase (RN2), the conductivities σ_A (blue) and σ_B (red) do not differ, as long as we choose to source the background at the same $\mu_A = \mu_B$. The width Γ (rate of momentum dissipation) is greater for RN1 than for RN2 at the same $T/\mu_A = 0.099$.

4.4 Two-Charge phase transition and the two-fluid

For a fixed μ_A we can decrease the temperature of the system by increasing μ_B adiabatically, until ϕ will condense and we again get the spontaneous transition into the

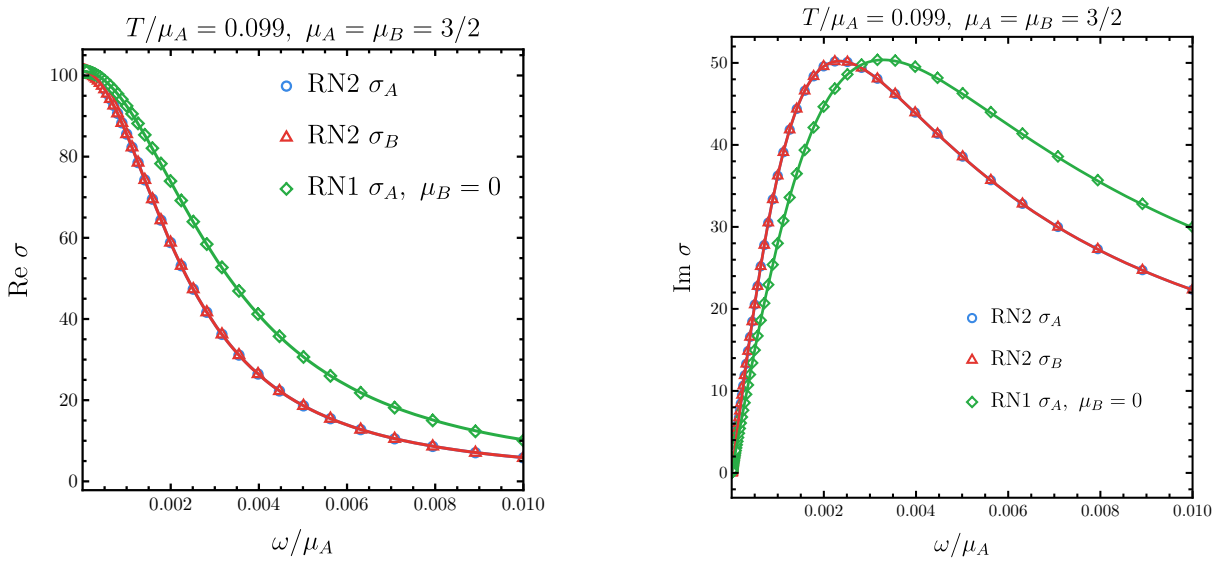

(a) ***(b)***

Figure 4.1: RN2 conductivity compared to RN1 at constant $\mathbf{T}/\mu$. *(a) Real and (b) imaginary part of conduvtivies in the RN2 system compared to RN1. The index* σ_X *indicates which field was sourced at the boundary and which conductivity measured, see Eqs.* (4.24),(4.25). *The blue curves are exactly covered by the red.* $\mu_A = 1.77$ *to tune to the same ratio* $T/\mu_A = 0.099$. *RN1 is fitted with* $\omega_p^2 = 0.479,\ \Gamma = 0.0066,\ \sigma_Q = 0.535$ *and RN2 with* $\omega_p^2 = 0.353,\ \Gamma = 0.0035,\ \sigma_Q = 0.624$ *to Eqs.* (1.36),(1.37).

	ω_p^2	Γ	σ_s
RN2 A (blue)	0.194	0.00037	$-2.3 \cdot 10^{-9}$
RN2 B (red)	0.213	0.00037	$-2.4 \cdot 10^{-9}$
SC2 A (green)	0.211	0.00035	$3.6 \cdot 10^{-10}$
SC2 B (yellow)	0.197	0.00035	-0.018

Table 4.1: Two-fluid fitting parameters of the RN2/SC2 conductivities. *Parameters used for fitting the curves of Figs. 4.3 to the two-fluid conductivity Eq.* (3.12).

superconducting phase without explicitly sourcing the boundary operator, as is shown in Fig. 4.2. The critical temperature with respect to the source T/μ_B decreased from 0.157 in SC1 to 0.132 in SC2. Adding another charge to the system decreases the temperature and therefore also the critical temperature. One could investigate further what influence μ_A has on the phase transition, but this is again not our main focus. Even at temperatures below T_C, the RN2 phase is still a solution to the equations of motion. It is, however, energetically less favourable and therefore more unstable. One can, via the temperature, calculate the free energy and show that the SC solution has the lower free energy at those temperatures. We can still compare the RN2 conductivity to the SC2 conductivity at the same temperature T/μ_A. We do this by either hand-selecting the numerical solution we get at low T by setting $\chi = \phi = 0$ (no superconductor) or by using the analytical background solution that comes without χ and ϕ in the first place.

The resulting optical conductivities σ_A and σ_B of the condensed SC2 compared to RN2 system are shown in Fig. 4.3. Qualitatively, all curves behave the same way as in the separate RN1 and SC1 systems. A non-zero β/μ_A leads to translational symmetry

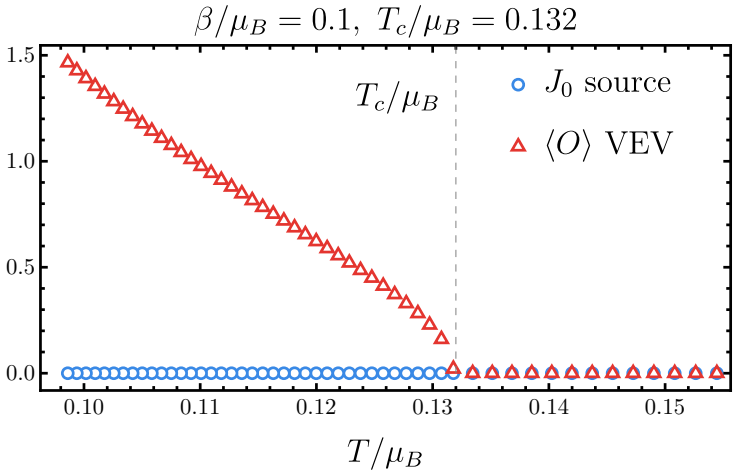

Figure 4.2: Phase transition from RN2 to SC2. *Phase transition of $\langle O \rangle$ without explicitly sourcing O. The critical temperature in units of the chemical potential of the second gauge potential B_t is $T_c/\mu_B = 0.157$. The other physical parameter $\beta/\mu_B = 0.1$ is kept constant. We are considering standard quantisation, where $m^2 = -2$ and $q = 3$.*

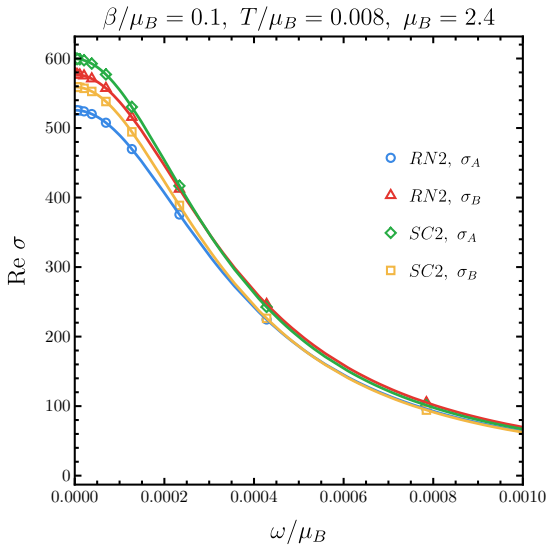

(a) *Now the two RN2 conductivities do not overlap, as $\mu_A \neq \mu_B$ in the RN background.*

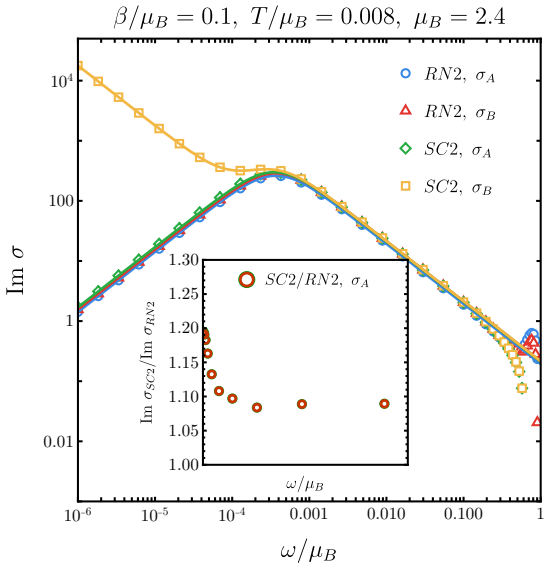

(b) *In the condensed phase, σ_B (yellow) again exhibits two-fluid behaviour of a δ in $\omega = 0$.*

Figure 4.3: Optical conductivities σ_A, σ_B of the RN2 and SC2 systems. *The (a) real and (b) imaginary part of the optical conductivity for low ω/μ_A is shown for different sourcings of RN2 and SC2. The SC background is at equal $\mu_A = \mu_B = 2.4$. The RN is background at $\mu_A = 2.29$, $\mu_B = 2.4$ to keep $T/\mu_B = 0.008$. The parameters fitting to Eq. (3.13) are given in Tab. 4.1.*

breaking and a finite-Γ Lorentzian in the real and imaginary parts. The superconductor is best described by a two-fluid model – one part normal, one part superfluid. An important point being, that even though there is a holographic superconductor present in the SC2 case, when measuring σ_A in Fig. 4.3 (green), we do not get a δ-peak of infinite conductivity. This is because, as we have repeated, the A-system is not coupled to an unstable scalar field and therefore remains an RN metal at all temperatures. All curves, be it fitting to a simple Drude or to the two-fluid model, deviate from their fit for $\omega \geq \mu_A$, where they slowly approach the behaviour of the zero density, that is zero μ_A, μ_B CFT. The fitting parameters in Tab. 4.1 underline the appearance of the $\sigma_s/i\omega$ term with condensation in the σ_B conductivity, while the rate of momentum dissipation Γ decreases almost not notably. The impact of the condensation on the height σ_0 of the Lorentzian of σ_A is exactly what we were looking for. As seen in the previous chapter, we expect the DC-value of the real part (proportional to σ_0) to decrease with condensation. This clearly happens for the B-conductivity. This can be seen both from the change of the red and yellow curves in Figs. 4.3 or by the change in σ_0 in Tab. 4.1.

In the A-system, however, we see no such inversion of relationship with condensation, that is, both the real and imaginary part of σ_A are greater when ϕ is condensed. Further investigation could be made whether this impact comes from the translational symmetry breaking parameter β or whether there is a fundamental difference when considering the two-charge rather than the one-charge system of Figs. 3.4.

Conclusion

The goal of this work was twofold: firstly, exploring the AdS/CFT duality and with it well-known holographic models like the Reissner-Nordström metal and the holographic superconductor, to then become familiar with the numerical techniques to describe them. Secondly, fusing the two explored models into a new setup with the hope of seeing low energy excitations missing so far in the standard RN setup.

The brief theoretical framework for the duality and basics of Drude conductivity of the first chapter is by far not exhaustive, but gives a solid foundation on which holographic systems can be investigated and which could easily be expanded upon. On the example of the thoroughly studied Reissner-Nordström metal we were able to set up and test the impact of translational symmetry breaking and calculate the optical conductivity. Comparing to closed expressions derived in other studies, we could verify our methods quantitatively, gaining some reassurance on the numerical methods for obtaining transport properties applied.

We studied the Hartnoll, Herzog and Horowitz model of the holographic equivalent of a superconductor in detail. Due to the lack of a closed description of the static background, we managed to instead numerically solve for it. Not only were we able to see the phase transition and study its impact on the system's temperature and spectral density, we also succeeded in reproducing the two-fluid model of a relaxed superconductor, where normal and superfluid parts coexist.

Finally, bringing the basics together with the RN and superconducting phase, we managed to construct a model comprising of a metal that stays normal at any temperature with one that transitions into a superconductor: the two-charge holographic superconductor. Here again, we managed to numerically obtain the background with its black hole temperature and the optical conductivity. To reduce the degrees of freedom for solving the system and to transform into more universal variables, we re-expressed our system with respect to certain gauge invariant variables of the spin 1 sector. Most notably, does the two-fluid behaviour persist in the two-charge holographic superconductor only for the superconductor's conductivity while the conductivity of the RN system remains normal at all temperatures. The condensation however, does impact the spectral density of the RN system.

An outlook and suggestion for future work would be to also consider the spin 0 sector, which includes fluctuations of the condensed scalar field's phase. There we suspect low energy excitations to appear with condensation, signalling the appearance of phonons in the boundary that would improve upon the applicability of the basic RN system.

Bibliography

[1] Juan M. Maldacena. "The Large N Limit of Superconformal Field Theories and Supergravity". In: *International Journal of Theoretical Physics* 38.4 (1999), pp. 1113–1133. ISSN: 00207748. DOI: 10.1023/A:1026654312961. arXiv: hep-th/9711200.

[2] S. S. Gubser, I. R. Klebanov, and A. M. Polyakov. "Gauge Theory Correlators from Non-Critical String Theory". In: *Physics Letters B* 428.1 (May 1998), pp. 105–114. ISSN: 03702693. DOI: 10.1016/S0370-2693(98)00377-3. arXiv: hep-th/9802109.

[3] Edward Witten. *Anti De Sitter Space And Holography*. Apr. 6, 1998. arXiv: hep-th/9802150.

[4] E. V. Shuryak. "What RHIC Experiments and Theory tell us about Properties of Quark-Gluon Plasma ?" In: *Nuclear Physics A* 750.1 (Mar. 2005), pp. 64–83. ISSN: 03759474. DOI: 10.1016/j.nuclphysa.2004.10.022. arXiv: hep-ph/0405066.

[5] Sean A. Hartnoll, Christopher P. Herzog, and Gary T. Horowitz. "Building an AdS/CFT superconductor". In: *Physical Review Letters* 101.3 (July 14, 2008), p. 031601. ISSN: 0031-9007, 1079-7114. DOI: 10.1103/PhysRevLett.101.031601. arXiv: 0803.3295[cond-mat,physics:gr-qc,physics:hep-th].

[6] Gary T. Horowitz, Jorge E. Santos, and David Tong. "Optical Conductivity with Holographic Lattices". In: *Journal of High Energy Physics* 2012.7 (July 2012), p. 168. ISSN: 1029-8479. DOI: 10.1007/JHEP07(2012)168. arXiv: 1204.0519[cond-mat,physics:hep-th].

[7] Gary T. Horowitz, Jorge E. Santos, and David Tong. "Further Evidence for Lattice-Induced Scaling". In: *Journal of High Energy Physics* 2012.11 (Nov. 2012), p. 102. ISSN: 1029-8479. DOI: 10.1007/JHEP11(2012)102. arXiv: 1209.1098[cond-mat,physics:hep-th].

[8] D. Tong. "Holographic Conductivity". In: *Acta Physica Polonica B* 44.12 (2013), p. 2579. ISSN: 0587-4254, 1509-5770. DOI: 10.5506/APhysPolB.44.2579.

[9] Jan Zaanen et al. *Holographic duality in condensed matter physics*. Cambridge: Cambridge University Press, 2015. 573 pp. ISBN: 978-1-107-08008-9.

[10] Floris Balm. "Translational symmetry breaking in holographic strange metals". Retrieved from https://hdl.handle.net/1887/3618303. PhD thesis. Delft-Leiden: Leiden University, May 2023.

[11] G. Policastro, D. T. Son, and A. O. Starinets. "Shear viscosity of strongly coupled N=4 supersymmetric Yang-Mills plasma". In: *Physical Review Letters* 87.8 (Aug. 2, 2001), p. 081601. ISSN: 0031-9007, 1079-7114. DOI: 10.1103/PhysRevLett.87.081601. arXiv: hep-th/0104066.

[12] Oscar J. C. Dias, Jorge E. Santos, and Benson Way. "Numerical Methods for Finding Stationary Gravitational Solutions". In: *Classical and Quantum Gravity* 33.13 (July 7, 2016), p. 133001. ISSN: 0264-9381, 1361-6382. DOI: 10.1088/0264-9381/33/13/133001. arXiv: 1510.02804[gr-qc,physics:hep-th].

[13] Nicolas Chagnet. "Applications of AdS/CFT to strongly correlated matter: from numerics to experiments". Retrieved from https://hdl.handle.net/1887/3762182. PhD thesis. Leiden: Leiden University, June 2024.

[14] Floris Balm et al. "T-linear resistivity, optical conductivity and Planckian transport for a holographic local quantum critical metal in a periodic potential". In: *Physical Review B* 108.12 (Sept. 26, 2023), p. 125145. ISSN: 2469-9950, 2469-9969. DOI: 10.1103/PhysRevB.108.125145. arXiv: 2211.05492[cond-mat,physics:hep-th].

[15] Tomas Andrade and Benjamin Withers. "A simple holographic model of momentum relaxation". In: *Journal of High Energy Physics* 2014.5 (May 2014), p. 101. ISSN: 1029-8479. DOI: 10.1007/JHEP05(2014)101. arXiv: 1311.5157[hep-th].

[16] Keun-Young Kim, Kyung Kiu Kim, and Miok Park. "A Simple Holographic Superconductor with Momentum Relaxation". In: *Journal of High Energy Physics* 2015.4 (Apr. 2015), p. 152. ISSN: 1029-8479. DOI: 10.1007/JHEP04(2015)152. arXiv: 1501.00446[cond-mat,physics:hep-th].

[17] Igor R. Klebanov and Juan M. Maldacena. "Solving quantum field theories via curved spacetimes". In: *Physics Today* 62.1 (Jan. 1, 2009), pp. 28–33. ISSN: 0031-9228, 1945-0699. DOI: 10.1063/1.3074260.

[18] Joshua D. Qualls. *Lectures on Conformal Field Theory*. May 19, 2016. arXiv: 1511.04074[hep-th].

[19] Nigel Goldenfeld. *Lectures on phase transitions and the renormalization group*. Frontiers in physics v. 85. Reading, Mass: Addison-Wesley, Advanced Book Program, 1992. 394 pp. ISBN: 978-0-201-55409-0 978-0-201-55408-3.

[20] Mikio Nakahara. *Geometry, topology, and physics*. 2nd ed. Graduate student series in physics. OCLC: ocm52622950. Bristol ; Philadelphia: Institute of Physics Publishing, 2003. 573 pp. ISBN: 978-0-7503-0606-5.

[21] Sean M. Carroll. *Spacetime and geometry: an introduction to general relativity*. Nachdr. San Francisco Munich: Addison-Wesley. 513 pp. ISBN: 978-0-8053-8732-2.

[22] John McGreevy. "Holographic duality with a view toward many-body physics". In: *Advances in High Energy Physics* 2010.1 (Jan. 2010), p. 723105. ISSN: 1687-7357, 1687-7365. DOI: 10.1155/2010/723105. arXiv: 0909.0518[cond-mat,physics:hep-th].

[23] Matteo Baggioli. *A Practical Mini-Course on Applied Holography*. 2019. DOI: 10.1007/978-3-030-35184-7. arXiv: 1908.02667[cond-mat,physics:hep-ph,physics:hep-th].

[24] Sean A. Hartnoll, Andrew Lucas, and Subir Sachdev. *Holographic quantum matter*. Mar. 20, 2018. arXiv: 1612.07324[cond-mat,physics:hep-th].

[25] Sean A. Hartnoll. *Lectures on holographic methods for condensed matter physics*. Jan. 17, 2010. DOI: 10.1088/0264-9381/26/22/224002. arXiv: 0903.3246[cond-mat,physics:hep-th].

[26] O. Aharony et al. "Large N Field Theories, String Theory and Gravity". In: *Physics Reports* 323.3 (Jan. 2000), pp. 183–386. ISSN: 03701573. DOI: 10.1016/S0370-1573(99)00083-6. arXiv: hep-th/9905111.

[27] Neil W. Ashcroft and N. David Mermin. *Solid state physics*. New York: Holt, Rinehart and Winston, 1976. 826 pp. ISBN: 978-0-03-083993-1.

[28] Alexander Altland and Ben D. Simons. *Condensed matter field theory*. 2. ed., [repr.] Cambridge: Cambridge Univ. Press, 2012. 770 pp. ISBN: 978-0-521-76975-4.

[29] D. T. Son and A. O. Starinets. "Minkowski-space correlators in AdS/CFT correspondence: recipe and applications". In: *Journal of High Energy Physics* 2002.9 (Sept. 19, 2002), pp. 042–042. ISSN: 1029-8479. DOI: 10.1088/1126-6708/2002/09/042. arXiv: hep-th/0205051.

[30] Richard A. Davison, Blaise Goutéraux, and Sean A. Hartnoll. "Incoherent transport in clean quantum critical metals". In: *Journal of High Energy Physics* 2015.10 (Oct. 2015), p. 112. ISSN: 1029-8479. DOI: 10.1007/JHEP10(2015)112. arXiv: 1507.07137[cond-mat,physics:hep-th].

[31] Z. Q. Li et al. "Dirac charge dynamics in graphene by infrared spectroscopy". In: *Nature Physics* 4.7 (July 2008), pp. 532–535. ISSN: 1745-2473, 1745-2481. DOI: 10.1038/nphys989.

[32] Tomas Andrade. *Holographic Lattices and Numerical Techniques*. Dec. 12, 2017. arXiv: 1712.00548[gr-qc,physics:hep-th].

[33] Aristomenis Donos and Jerome P. Gauntlett. "Minimally packed phases in holography". In: *Journal of High Energy Physics* 2016.3 (Mar. 2016), p. 148. ISSN: 1029-8479. DOI: 10.1007/JHEP03(2016)148. arXiv: 1512.06861[hep-th].

[34] Sean A. Hartnoll, Christopher P. Herzog, and Gary T. Horowitz. *Holographic Superconductors*. Oct. 8, 2008. DOI: 10.1088/1126-6708/2008/12/015. arXiv: 0810.1563[hep-th].

[35] Tomas Andrade and Simon A. Gentle. *Relaxed superconductors*. Apr. 23, 2015. arXiv: 1412.6521[hep-th].

[36] Gary T. Horowitz and Matthew M. Roberts. "Zero Temperature Limit of Holographic Superconductors". In: *Journal of High Energy Physics* 2009.11 (Nov. 5, 2009), pp. 015–015. ISSN: 1029-8479. DOI: 10.1088/1126-6708/2009/11/015. arXiv: 0908.3677[cond-mat,physics:gr-qc,physics:hep-th].

[37] Hyun-Sik Jeong et al. "Collective dynamics and the Anderson-Higgs mechanism in a bona fide holographic superconductor". In: *Journal of High Energy Physics* 2023.3 (Mar. 27, 2023), p. 206. ISSN: 1029-8479. DOI: 10.1007/JHEP03(2023)206. arXiv: 2302.02364[hep-th].

[38] Peter Breitenlohner and Daniel Z. Freedman. "Positive energy in anti-de Sitter backgrounds and gauged extended supergravity". In: *Physics Letters B* 115.3 (Sept. 1982), pp. 197–201. ISSN: 03702693. DOI: 10.1016/0370-2693(82)90643-8.

[39] Navid Abbasi and Sara Tahery. "Complexified quasinormal modes and the pole-skipping in a holographic system at finite chemical potential". In: *Journal of High Energy Physics* 2020.10 (Oct. 2020), p. 76. ISSN: 1029-8479. DOI: 10.1007/JHEP10(2020)076. arXiv: 2007.10024[hep-th,physics:nucl-th].

Appendix A

Gauge invariant variables and equations of motion

The gauge invariant equations of motion for the spin 1 gauge independent variables of Eq. (4.15) are

$$\begin{aligned} 0 = {} & \mathcal{A}'' + \mathcal{A}' \frac{-12 + 2z^2\beta^2 + 12f - 4z^2\phi^2 + e^{\chi} z^4 (A_t')^2 + e^{\chi} z^4 (B_t')^2}{4zf} \\ & + \mathcal{A} \frac{e^{\chi}\omega^2 \left(e^{\chi}\omega^2 - f\left(\beta^2 + e^{\chi} z^2 (A_t')^2\right)\right)}{f^2 \left(e^{\chi}\omega^2 - \beta^2 f\right)} - \mathcal{B} \frac{e^{2\chi} z^2 \omega^2 A_t' B_t'}{e^{\chi}\omega^2 f - \beta^2 f^2} - \mathcal{D}' \frac{e^{\chi}\beta^2 A_t'}{e^{\chi}\omega^2 - \beta^2 f}, \end{aligned} \tag{A.1}$$

$$\begin{aligned} 0 = {} & \mathcal{B}'' + \mathcal{B}' \frac{\left(z^4 e^{\chi} (A_t')^2 + z^4 e^{\chi} (B_t')^2 + 12f + 2\beta^2 z^2 - 4z^2\phi^2 - 12\right)}{4zf} \\ & + \mathcal{B} \frac{\left(f\left(-\frac{\omega^2 z^2 e^{2\chi} (B_t')^2}{\omega^2 e^{\chi} - \beta^2 f} - 2\phi^2\right) + \omega^2 e^{\chi}\right)}{f^2} - \mathcal{A} \frac{\omega^2 z^2 e^{2\chi} A_t' B_t'}{\omega^2 f e^{\chi} - \beta^2 f^2} - \mathcal{D}' \frac{\beta^2 e^{\chi} B_t'}{\omega^2 e^{\chi} - \beta^2 f} \end{aligned} \tag{A.2}$$

$$\begin{aligned} 0 = {} & \mathcal{D}'' + \frac{\omega^2 z \mathcal{A} e^{\chi} A_t' \left(f\left(z^4 e^{\chi} (A_t')^2 + z^4 e^{\chi} (B_t')^2 + 2\beta^2 z^2 - 4z^2\phi^2 - 12\right)\right)}{4f^2 \left(\omega^2 e^{\chi} - \beta^2 f\right)} \\ & + \frac{-2z^4 B_t^2 e^{\chi}\phi^2 - 2f^2 \left(z^4\phi'^2 + 2z^3\phi\phi' + z^2\phi^2 - 6\right)}{4f^2 \left(\omega^2 e^{\chi} - \beta^2 f\right)} \\ & + \mathcal{B} \frac{-\omega^2 f e^{\chi} B_t' z \left(z^4 e^{\chi} (A_t')^2 + z^4 e^{\chi} (B_t')^2 - 2f\left(z^4\phi'^2 + 2z^3\phi\phi' + z^2\phi^2 - 6\right) + 2\beta^2 z^2 - 4z^2\phi^2 - 12\right)}{4f^2 \left(\beta^2 f - \omega^2 e^{\chi}\right)} \\ & + \frac{+2z\omega^2 z^4 B_t^2 e^{2\chi}\phi^2 B_t' + 8z B_t f z\phi^2 \left(\beta^2 f - \omega^2 e^{\chi}\right)}{4f^2 \left(\beta^2 f - \omega^2 e^{\chi}\right)} \\ & + \mathcal{D}' \frac{e^{\chi}\left(2\phi^2 \left(\beta^2 z^4 B_t^2 + 2\omega^2 z^2\right) - \omega^2 \left(z^4 e^{\chi} (A_t')^2 + z^4 e^{\chi} (B_t')^2 + 2\beta^2 z^2 - 12\right)\right)}{4zf \left(\beta^2 f - \omega^2 e^{\chi}\right)} \\ & + \frac{+2\beta^2 f^2 \left(z^4\phi'^2 + 2z^3\phi\phi' + z^2\phi^2 - 4\right) - 4\omega^2 f e^{\chi}}{4zf \left(\beta^2 f - \omega^2 e^{\chi}\right)} + z^2 A_t' \mathcal{A}' + z^2 B_t' \mathcal{B}' \\ & + \frac{\mathcal{D}\left(\omega^2 e^{\chi} - \beta^2 f\right)}{f^2} \end{aligned} \tag{A.3}$$

Analogously, for spin 0 we get the gauge independent variables

$$\left\{\mathcal{V} = a_x,\ \mathcal{W} = b_x,\ \mathcal{X} = h_{xx} - h_{yy},\ \mathcal{Y} = \frac{\varphi}{z} + \frac{h_{yy}}{2z}(\phi + z\phi'),\ \mathcal{Z} = h_{tx} + \frac{i\omega}{\beta}\psi_x\right\}. \quad \text{(A.4)}$$

The equations depending solely on these variables have not been readily derived by the time of finishing this work. This could be a next step in getting a better understanding of the system and its longitudinal spin 0 sector.